State of the Global Climate 2020

PROVISIONAL REPORT

WEATHER CLIMATE WATER

WORLD METEOROLOGICAL ORGANIZATION

Forest Fire, Sakha Republic, Russia, June 2021 – Copernicus Sentinel / Sentinel Hub / Pierre Markuse

State of the Global Climate 2020
-Provisional report-

Key messages

Concentrations of the major greenhouse gases, CO_2, CH_4, and N_2O, continued to increase in 2019 and 2020.

Despite developing La Niña conditions, global mean temperature in 2020 is on course to be one of the three warmest on record. The past six years, including 2020, are likely to be the six warmest years on record.

Sea level has increased throughout the altimeter record, but recently sea level has risen at a higher rate due partly to increased melting of ice sheets in Greenland and Antarctica. Global mean sea level in 2020 was similar to that in 2019 and both are consistent with the long-term trend. A small drop in global sea level in the latter part of 2020 is likely associated with developing La Niña conditions, similar to the temporary drops associated with previous La Niña events.

Over 80% of the ocean area experienced at least one marine heatwave in 2020 to date. More of the ocean experienced marine heat waves classified as 'strong' (43%) than 'moderate' (28%).

2019 saw the highest ocean heat content on record and the rate of warming over the past decade was higher than the long-term average, indicating continued uptake of heat from the radiative imbalance caused by greenhouse gases.

In the Arctic, the annual minimum sea-ice extent was the second lowest on record and record low sea-ice extents were observed in the months of July and October. Antarctic sea ice extent remained close to the long-term average.

The Greenland ice sheet continued to lose mass. Although the surface mass balance was close to the long-term average, loss of ice due to iceberg calving was at the high end of the 40-year satellite record. In total, approximately 152 Gt of ice were lost from the ice sheet between September 2019 and August 2020.

Heavy rain and extensive flooding occurred over large parts of Africa and Asia in 2020. Heavy rain and flooding affected much of the Sahel, the Greater Horn of Africa, the India subcontinent and neighbouring areas, China, Korea and Japan, and parts of southeast Asia at various times of the year.

With 30 named storms (as of 17 November) the north Atlantic hurricane season had its largest number of named storms on record with a record number making landfall in the United States of America. The last storm of the season (to date) Iota, was also the most intense, reaching category 5.

Tropical storm activity in other basins was near or below the long-term mean, although there were severe impacts.

Severe drought affected many parts of interior South America in 2020, with the worst-affected areas being northern Argentina, Paraguay and western border areas of Brazil. Estimated agricultural losses were near US$3 billion in Brazil with additional losses in Argentina, Uruguay and Paraguay.

Climate and weather events have triggered significant population movements and have severely affected vulnerable people on the move, including in the Pacific region and Central America.

Global climate indicators

Global Climate Indicators[1] describe the changing climate, providing a broad view of the climate at a global scale. They are used to monitor the domains most relevant to climate change, including the composition of the atmosphere, the energy changes that arise from the accumulation of greenhouse gases and other factors, as well as the responses of land, ocean and ice. Details on the data sets used in each section can be found at the end of the report.

Temperature

The global mean temperature for 2020 (January to October) was 1.2 ± 0.1 °C above the 1850–1900 baseline, used as an approximation of pre-industrial levels (Figure 1). 2020 is likely to be one of the three warmest years on record globally. The WMO assessment is based on five global temperature datasets (Figure 1). All five of those data sets currently place 2020 as 2nd warmest for the year to date when compared to equivalent periods in the past (January to October). However, the difference between the top three years is small and exact rankings for each data set could change once the year is complete. The spread of the five estimates for the January to October average is between 1.11 °C and 1.23 °C.
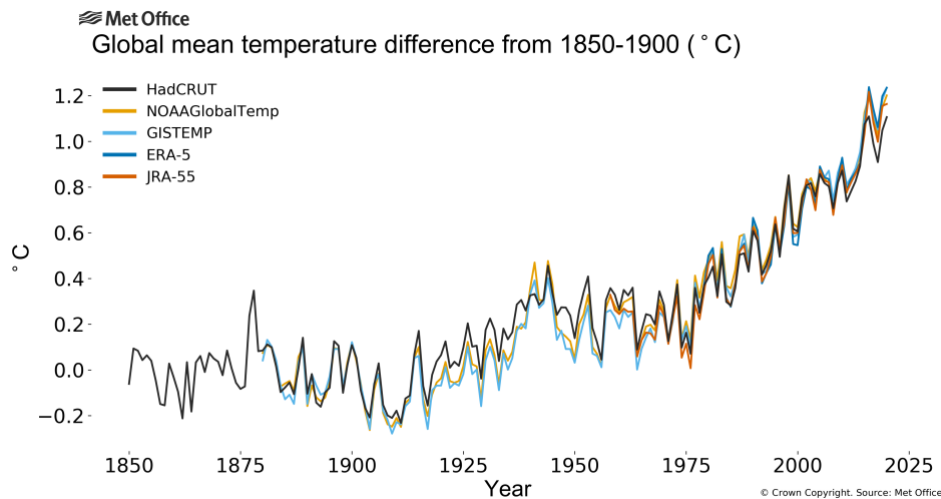

Figure 1: Global annual mean temperature difference from preindustrial conditions (1850–1900). The two reanalyses (ERA5 and JRA-55) are aligned with the in situ datasets (HadCRUT, NOAAGlobalTemp and GISTEMP) over the period 1981–2010. Data for 2020 run from January to October.

---

[1] https://gcos.wmo.int/en/global-climate-indicators

The warmest year on record to date, 2016, began with an exceptionally strong El Niño, a phenomenon which contributes to elevated global temperatures. Despite neutral or comparatively weak El Niño conditions early in 2020[2], and La Niña conditions developing by late September[3], the warmth of 2020 is comparable to that of 2016.

With 2020 on course to be one of the three warmest years on record, the past six years, 2015–2020, are likely to be the six warmest on record. The last five-year (2016–2020) and 10-year (2011–2020) averages are also the warmest on record.

Although the overall warmth of the year is clear, there were variations in temperature anomalies across the globe (Figure 2). While most land areas were warmer than the long-term (1981-2010) average, one area in northern Eurasia stands out with temperatures more than five degrees above average for the first 10 months of the year (see: Sidebar**: The Arctic in 2020**). Other notable areas of warmth include limited areas of the southwestern United States, northern and western parts of South America, parts of Central America, and wider areas of Eurasia including parts of China. For Europe, it was the warmest January to October period on record. Areas of below-average temperature on land included western Canada, limited areas of Brazil, northern India and south-eastern Australia.
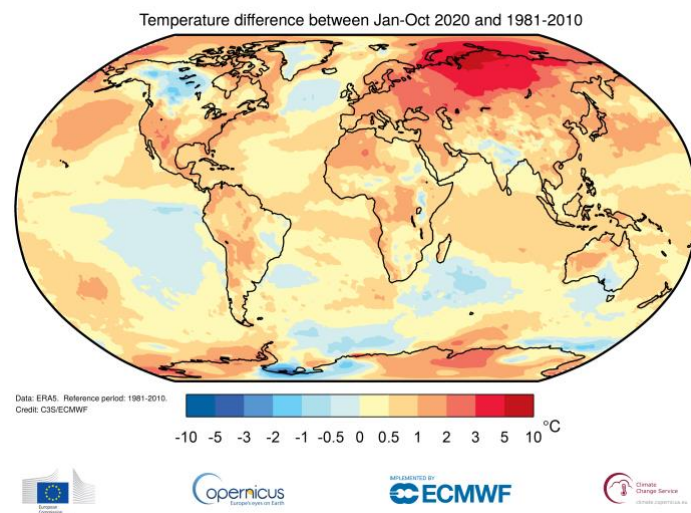

Figure 2: Temperature anomalies relative to the 1981-2010 long-term average from the ERA5 reanalysis for January to October 2020. Credit: Copernicus Climate Change Service, ECMWF.

Greenhouse gases and stratospheric ozone

Atmospheric concentrations of greenhouse gases reflect a balance between emissions from human activities, natural sources and biospheric and oceanic sinks. Increasing levels of greenhouse gases in the atmosphere due to human activities are the major driver of climate change since the mid-20th century.

Global averaged mole fractions of greenhouse gases are calculated from *in situ* observations from multiple sites in the Global Atmosphere Watch Programme of WMO and partner networks. These data are available from the World Data Centre for Greenhouse Gases operated by Japan Meteorological Agency[4].

---

[2] https://origin.cpc.ncep.noaa.gov/products/analysis_monitoring/ensostuff/ONI_v5.php
[3] http://www.bom.gov.au/climate/enso/wrap-up/archive/20200929.archive.shtml
[4] https://gaw.kishou.go.jp/

In 2019, greenhouse gas concentrations reached new highs (Figure 3), with globally averaged mole fractions of carbon dioxide (CO_2) at 410.5±0.2 parts per million (ppm), methane (CH_4) at 1877±2 parts per billion (ppb) and nitrous oxide (N_2O) at 332.0±0.1 ppb. These values constitute, respectively, 148%, 260% and 123% of pre-industrial (before 1750) levels. The increase in CO_2 from 2018 to 2019 (2.6 ppm) was larger than both the increase from 2017 to 2018 (2.3 ppm) and the average over the last decade (2.37 ppm per year). For CH_4, the increase from 2018 to 2019 was slightly lower than from 2017 to 2018 but still higher than the average over the last decade. For N_2O, the increase from 2018 to 2019 was also lower than that observed from 2017 to 2018 and practically equal to the average growth rate over the past 10 years.

The temporary reduction in emissions in 2020 related to measures taken in response to COVID-19[5] is likely to lead to only a slight decrease in the annual growth rate of CO_2 concentration in the atmosphere, which will be practically indistinguishable from the natural interannual variability driven largely by the terrestrial biosphere. Real-time data from specific locations, including Mauna Loa (Hawaii) and Cape Grim (Tasmania) indicate that levels of CO_2, CH_4 and N_2O continued to increase in 2020.

The IPCC Special Report on Global Warming of 1.5 °C found that limiting warming to 1.5°C above pre-industrial levels implies reaching net zero CO_2 emissions globally around 2050 and concurrent deep reductions in emissions of non-CO_2 forcers.
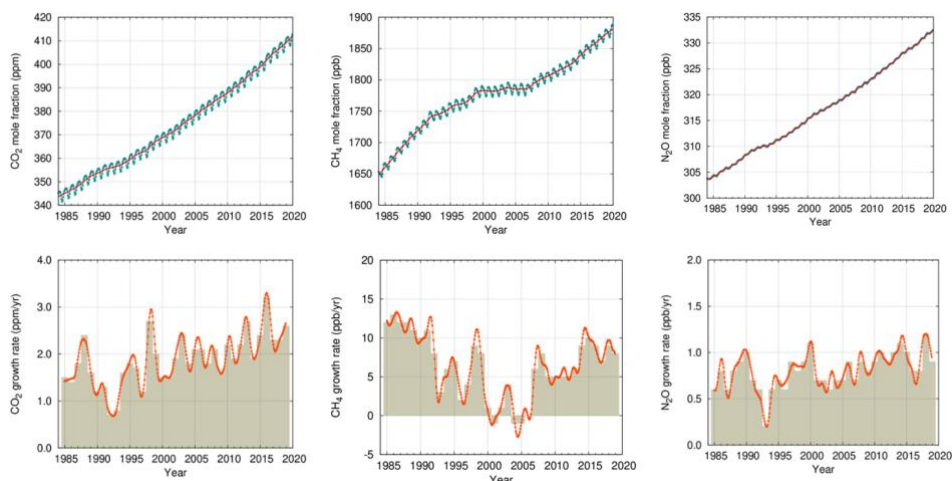

Figure 3: Top row: Globally averaged mole fraction (measure of concentration), from 1984 to 2019, of CO₂ in parts per million (left), CH₄ in parts per billion (centre) and N₂O in parts per billion (right). The red line is the monthly mean mole fraction with the seasonal variations removed; the blue dots and line show the monthly averages. Bottom row: the growth rates representing increases in successive annual means of mole fractions for CO₂ in parts per million per year are shown as grey columns (left), CH₄ in parts per billion per year (centre) and N₂O in parts per billion per year (right) (Source: WMO Global Atmosphere Watch).

Stratospheric ozone and ozone-depleting gases

Following the success of the Montreal Protocol, use of halons and CFCs has been reported as discontinued but their levels in the atmosphere continue to be monitored. Because of their long lifetime, these compounds will remain in the atmosphere for many decades and even if there were no new emissions, there is still more than enough chlorine and bromine present to cause complete destruction of ozone in Antarctica from August to December. As a result, the formation of the

---

[5] Liu, Z., Ciais, P., Deng, Z. *et al.* Near-real-time monitoring of global CO₂ emissions reveals the effects of the COVID-19 pandemic. *Nat Commun* **11,** 5172 (2020). https://doi.org/10.1038/s41467-020-18922-7

Antarctic ozone hole continues to be an annual spring event with year-to-year variation in its size and depth governed to a large degree by meteorological conditions.

The 2020 ozone hole developed relatively early and continued growing resulting in a large and deep ozone hole which, as of November 2020, has a larger than average (1979-2019 mean) area of ozone depletion and lower than average minimum ozone. The ozone hole area reached its maximum area for 2020 on 20 September at 24.8 million km^2, the same area as in 2018. The area of the hole was closer to the maxima observed in years such as 2015 (28.2 million km^2) and 2006 (29.6 million km^2) than 2019 (16.4 million km^2) according to an analysis from the National Aeronautics and Space Administration (NASA).

At the other end of the earth, unusual atmospheric conditions led to ozone concentrations over the Arctic falling to a record low for the month of March. Unusually weak "wave" events in the upper atmosphere left the polar vortex relatively undisturbed, preventing mixing of ozone-rich air from lower latitudes. In addition, the stratospheric polar vortex over the Arctic was strong and this, combined with consistently very low temperatures, allowed a large area of polar stratospheric clouds to grow. When the sun rises after the polar winter, it triggers chemical processes in the polar stratospheric clouds that lead to depletion of ozone. Measurements from weather balloons indicated ozone depletion surpassing the levels reported in 2011 and together with satellite observations point to stratospheric ozone levels down to around 205 Dobson Units on March 12, 2020. The typical lowest ozone values previously observed over the Arctic in March are at least 240 Dobson Units.

Ocean

The majority of the excess energy that accumulates in the earth system due to increasing concentrations of greenhouse gases is taken up by the ocean. The added energy warms the ocean and the consequent thermal expansion of the water leads to sea level rise. The surface ocean has warmed more rapidly than the interior and this can be seen in the rise of global mean temperature and also in the increased incidence of marine heatwaves. As the concentration of CO_2 in the atmosphere rises, so too does the concentration of CO_2 in the oceans. This affects ocean chemistry, lowering the average pH of the water, a process known as ocean acidification. All these changes have broad range of impacts in the oceans and coastal areas.

Ocean heat content

Increasing human emissions of CO_2 and other greenhouse gases cause a positive radiative imbalance at the top of the atmosphere – the Earth Energy Imbalance (EEI) - which is driving global warming through an accumulation of energy in the form of heat in the Earth system[6,7,8]. Ocean Heat Content (OHC) is a measure of this heat accumulation in the Earth system, as around 90% of it is stored in the ocean. A positive EEI signals that the Earth's climate system is still responding to the current forcing[9] and that more warming will occur even if the forcing does not increase further[10].

Historical measurements of subsurface temperature back to the 1940s mostly rely on shipboard measurement systems, which constrains the availability of subsurface temperature observations at a

[6] Hansen, J. et al. (2011). Earth's energy imbalance and implications. Atmospheric Chemistry and Physics. https://doi.org/10.5194/acp-11-13421-2011

[7] Rhein, M. et al. 2013. Climate change 2013: The physical science basis.

[8] von Schuckmann, K. et al. (2016). An imperative to monitor Earth's energy imbalance. In Nature Climate Change. https://doi.org/10.1038/nclimate2876

[9] Hansen, J. et al. (2005). Earth's Energy Imbalance: Confirmation and Implications. Science, 308(5727), 1431 LP – 1435. https://doi.org/10.1126/science.1110252

[10] Hansen, J. et al. (2017). Young people's burden: requirement of negative CO2 emissions. Earth Syst. Dynam., 8(3), 577–616. https://doi.org/10.5194/esd-8-577-2017

global scale and at depth[11]. With the deployment of the Argo network of autonomous profiling floats, which first achieved near-global coverage in 2006, it is now possible to routinely measure OHC changes down to a depth of 2000m[12,13].

Various research groups have developed estimates of global OHC. Although they all rely more or less on the same database, the estimates show differences arising from the various statistical treatments of data gaps, the choice of climatology and the approach used to account for instrumental biases[14,15]. A concerted effort has been established to provide an international view on the global evolution of ocean warming[16], and an update to 2019 is shown in Figure 4 and Figure 5. More details can be found in von Schuckmann et al. (2020).
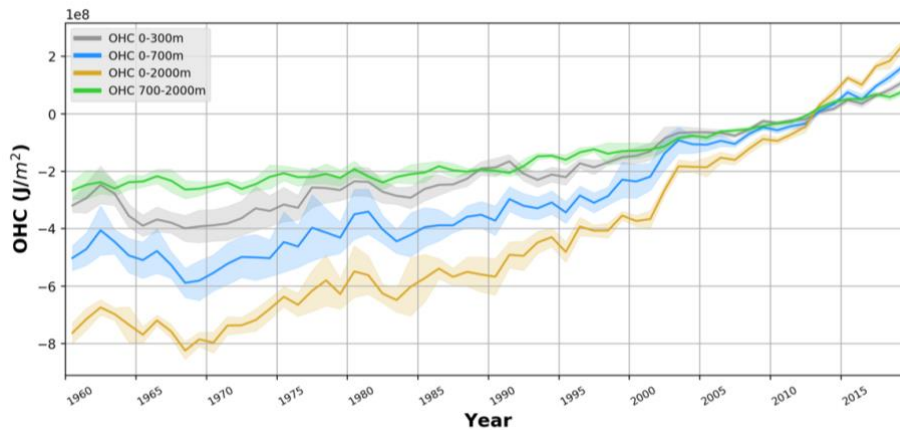

Figure 4: 1960-2019 ensemble mean time series and ensemble standard deviation (2-sigma, shaded) of global ocean heat content (OHC) anomalies relative to the 2005-2017 climatology for the 0-300m (grey), 0-700m (blue), 0-2000m (yellow) and 700-2000m depth layer (green). The ensemble mean is an outcome of a concerted international effort, and all products used are listed at the end of the report and in the legend of Figure 5. Note that values are given for the ocean surface area between 60°S-60°N, and limited to the 300m bathymetry of each product. Updated from von Schuckmann et al. (2020).

The 0-2000m depth layer of the global ocean continued to warm in 2019 reaching a new record high (Figure 4), and it is expected that it will continue to warm in the future[17]. Heat storage at intermediate depth (700-2000m) increased at a comparable rate to the 0-300m depth layer, which is in general agreement among the 15 international OHC estimates (Figure 5). All data sets agree that ocean warming rates show a particularly strong increase in the past two decades. Moreover, there is a clear indication that heat sequestration into the ocean below 700m depth took place over the past six decades linked to an increase of OHC trends over time. Ocean warming rates for the 0-2000m depth layer reached record rates of 1.2 (0.8) ± 0.2 Wm^{-2} for the ocean (global) area over the period

[11] Abraham, J. P. et al. (2013). A review of global ocean temperature observations: Implications for ocean heat content estimates and climate change. Reviews of Geophysics, 51(3), 450–483. https://doi.org/10.1002/rog.20022

[12] Riser, S. C. et al. (2016). Fifteen years of ocean observations with the global Argo array. Nature Climate Change, 6(2), 145–153. https://doi.org/10.1038/nclimate2872

[13] Roemmich, D. et al. (2019). On the Future of Argo: A Global, Full-Depth, Multi-Disciplinary Array. In Frontiers in Marine Science (Vol. 6, p. 439). https://www.frontiersin.org/article/10.3389/fmars.2019.00439

[14] Boyer, T. et al. (2016). Sensitivity of Global Upper-Ocean Heat Content Estimates to Mapping Methods, XBT Bias Corrections, and Baseline Climatologies. Journal of Climate, 29(13), 4817–4842. https://doi.org/10.1175/JCLI-D-15-0801.1

[15] von Schuckmann, K. et al. (2016). An imperative to monitor Earth's energy imbalance. In Nature Climate Change. https://doi.org/10.1038/nclimate2876

[16] von Schuckmann, K. et al. (2020). Heat stored in the Earth system: Where does the energy go? The GCOS Earth heat inventory team. Earth Syst. Sci. Data Discuss., 2020, 1–45. https://doi.org/10.5194/essd-2019-255

[17] IPCC, 2019: Summary for Policymakers. In: IPCC Special Report on the Ocean and Cryosphere in a Changing Climate[H.-O. Pörtner, D.C. Roberts, V. Masson-Delmotte, P. Zhai, M. Tignor, E. Poloczanska, K. Mintenbeck, A. Alegría, M. Nicolai, A. Okem, J. Petzold, B. Rama, N.M. Weyer (eds.)]. In press.

2010-2019. Below 2000m depth, the ocean also warmed albeit at the lower rate of 0.07 ± 0.04 Wm^{-2} from 1991-2018[18].
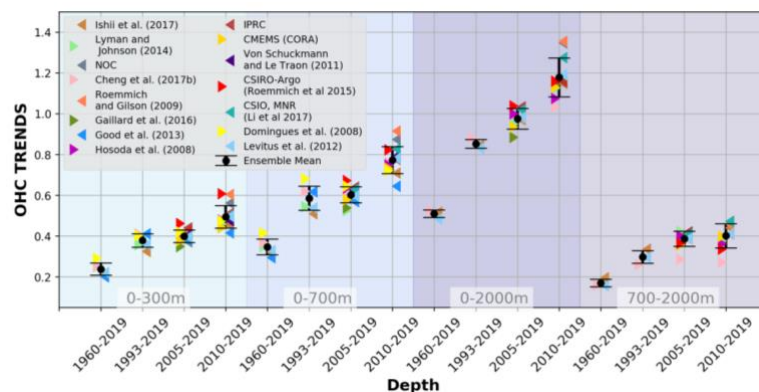

Figure 5: Linear trends of global ocean heat content (OHC) as derived from different temperature products (colors). References are provided at the end of the report. The ensemble mean and standard deviation (2-sigma) is given in black, respectively. The shaded areas show trends from different depth layer integrations, i.e. 0-300m (light turquoise), 0-700m (light blue), 0-2000m (purple) and 700-2000m (light purple). For each integration depth layer, trends are evaluated over four periods: historical (1960-2019), altimeter era (1993-2019), golden Argo era (2005-2019), and the most recent period 2010-2019. Updated from von Schuckmann et al. (2020).

Sea level

On average, since early 1993, the altimetry-based global mean rate of sea level rise amounts to 3.3 ± 0.3 mm/yr. The rate has also increased over that time. A greater loss of ice mass from the ice sheets is the main cause of the accelerated rise in the global mean sea level[19].

Global mean sea level in 2020 has been similar to that in 2019 (Figure *6*, left). A small decrease in the latter part of 2020 is likely related to La Niña conditions in the tropical Pacific. Interannual changes of global mean sea level around the long-term trend are correlated with ENSO variability (Figure *6*, right). During La Niña events, such as that in late 2020 and the strong La Niña of 2011, shifts in rainfall patterns transfer water mass from the ocean to tropical river basins on land, temporarily reducing global mean sea level. The opposite is observed during El Niño (e.g. the strong 2015-16 El Niño).

---

[18] Update from Purkey, S. G., and G. C. Johnson, 2010: Warming of Global Abyssal and Deep Southern Ocean Waters between the 1990s and 2000s: Contributions to Global Heat and Sea Level Rise Budgets. *J. Climate*, **23**, 6336–6351, https://doi.org/10.1175/2010JCLI3682.1.
[19] World Climate Research Programme (WCRP) Global Sea Level Budget Group, 2018: Global sea-level budget 1993–present. Earth System Science Data, 10, 1551–1590, https://doi.org/10.5194/essd-10-1551-2018.
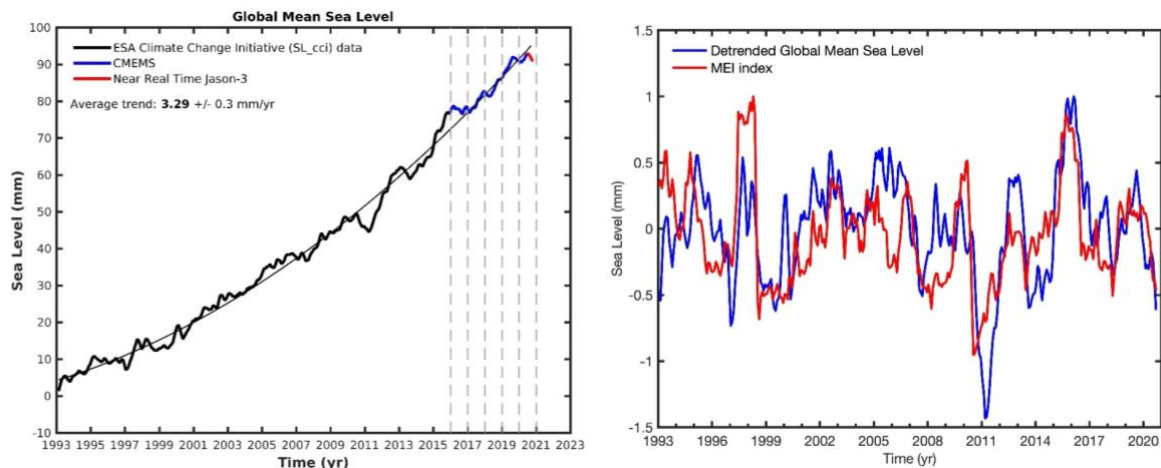
Figure 6: (left) Satellite altimetry-based global mean sea level for January 1993 to October 2020 (last data : 13 October 2020). Data from the ESA climate change Initiative sea level project, from January 1993 to December 2015, (thick black curve); extended by the Copernicus Marine and Environment Service, CMEMS, until August 2020 (blue curve) and with near real time altimetry data from the Jason-3 mission beyond August 2020 (red curve). The thin black curve is a quadratic function that best fits the data. Vertical dashed lines mark the start of each year from 2016 to 2021. (right) Interannual variability of the (with the quadratic function shown in left-hand panel subtracted) global mean sea level (blue curve) with the multivariate ENSO index (red curve) superimposed.

At a regional scale, sea level continues to rise non-uniformly. The strongest regional trends over the period January 1993 to January 2020 are seen in the southern hemisphere: east of Madagascar in the Indian Ocean; east of New Zealand in the Pacific Ocean; and east of Rio de la Plata/South America in the south Atlantic. An elongated eastward pattern is also seen in the north Pacific. A strong pattern that was seen in the western tropical Pacific over the first two decades of the altimetry record is now fading, suggesting that it was related to short-term variability. Regional sea level trends are dominated by variations in ocean heat content[20]. However, in some regions such as the Arctic, salinity changes due to freshwater input from the melting of ice on land play an important role.

Marine heatwaves

As with heatwaves on land, extreme heat can affect the near-surface layer of the oceans with a range of consequences for marine life and dependent communities. Satellite retrievals of sea-surface temperature can be used to monitor marine heatwaves (MHWs). MHWs are categorised here as Moderate, Strong, Severe or Extreme (for definitions see **Marine heatwave data**).

Much of the ocean experienced at least one 'Strong' MHW at some point in 2020 (Figure 7a). Conspicuously absent are MHWs in the Atlantic Ocean south of Greenland, and in the eastern equatorial Pacific. The Laptev Sea experienced an 'Extreme' MHW from June to October. Sea ice extent was unusually low in the region and adjacent land areas experienced heatwaves during the summer. Another important MHW to note in 2020 was the return of the semi-persistent warm region in the northeast Pacific. This event is similar in scale to the original 'blob'[21,22], which developed around 2013 with remnants lasting until 2016[23]. Approximately one fifth of the global

---

[20] IPCC, 2019: IPCC Special Report on the Ocean and Cryosphere in a Changing Climate [H.-O. Pörtner, D.C. Roberts, V. Masson-Delmotte, P. Zhai, M. Tignor, E. Poloczanska, K. Mintenbeck, A. Alegría, M. Nicolai, A. Okem, J. Petzold, B. Rama, N.M. Weyer (eds.)].

[21] Gentemann, C. L. et al., 2017: Satellite sea surface temperatures along the West Coast of the United States during the 2014 –2016 northeast Pacific marine heat wave. Geophysical Research Letters, 4 4, 312– 319, doi:10.1002 /2016GL071039.

[22] Di Lorenzo, E. and N. Mantua, 2016: Multi-year persistence of the 2014/15 North Pacific marine heatwave. Nature Climate Change, 6(11), p.1042, doi: 10.1038/nclimate308

[23] Schmeisser, L., Bond, N. A., Siedlecki, S. A., & Ackerman, T. P. (2019). The role of clouds and surface heat fluxes in the maintenance of the 2013–2016 Northeast Pacific Marine heatwave. Journal of Geophysical Research: Atmospheres, 124(20), 10772-10783.

ocean was experiencing a MHW on any given day in 2020 (Figure 7b). This is similar to 2019, but less than the 2016 peak of 23%. More of the ocean experienced MHWs classified as 'strong' (43%) than 'moderate' (28%). In total, 82% of the ocean experienced at least one MHW during 2020 (to date, Figure 7c), which is less than both 2019 (84%), and the 2016 peak (88%).
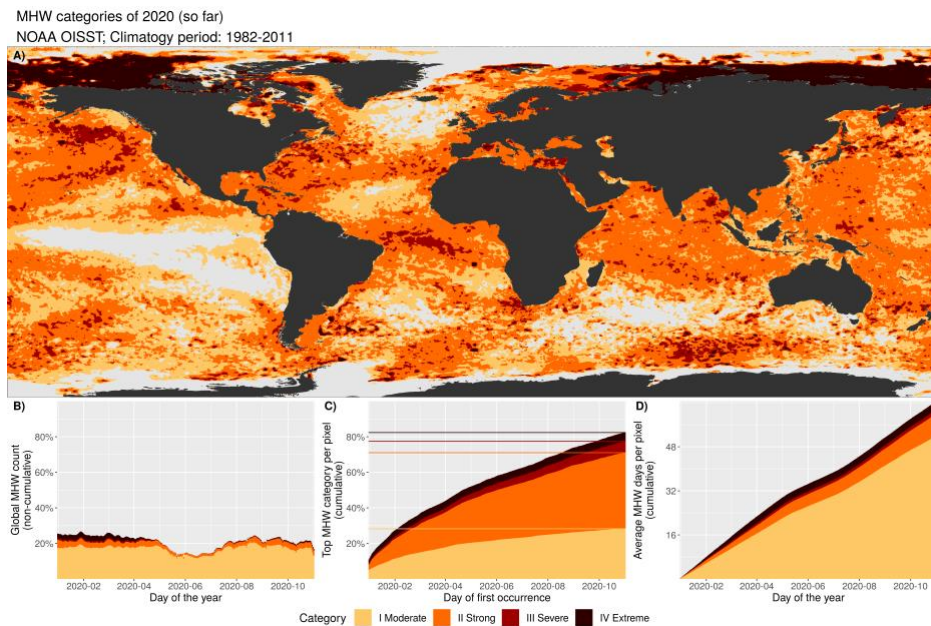

*Figure 7: (A) Global map showing the highest MHW category (for definitions see **Marine heatwave data**) experienced at each pixel over the course of the year, estimated using the NOAA OISST v2.1 dataset (reference period 1982–2011). Light grey indicates that no MHWs occurred in a pixel over the entire year; (B) Stacked bar plot showing the percentage of ocean pixels experiencing an MHW on any given day of the year; (C) Stacked bar plot showing the cumulative percentage of the ocean that experienced an MHW over the year[24].Horizontal lines in this figure show the final percentages for each category of MHW; (D) Stacked bar plot showing the cumulative number of MHW days averaged over all pixels in the ocean[25](Source: Robert Schlegel, IMEV).*

Ocean acidification

The ocean absorbs around 23% of the annual emissions of anthropogenic CO_2 to the atmosphere[26], thereby helping to alleviate the impacts of climate change on the planet[27]. The ecological costs of this process to the ocean are high, as the CO_2 reacts with seawater, lowering its pH, a process known as ocean acidification. Ocean acidification affects many organisms and ecosystem services, threatening food security by endangering fisheries and aquaculture. This is particularly a problem in the polar oceans because of the ocean chemistry of these cold regions. It also affects coastal protection by weakening coral reefs, which shield coastlines. As the acidity of the ocean increases, its capacity to absorb CO_2 from the atmosphere decreases, hampering the ocean's role in moderating climate change. Regular global observation and measurement of ocean acidification is needed to improve the understanding of its consequences, enable modelling and prediction of change and variability, and help inform mitigation and adaptation strategies.

Global efforts have been made to collect and compare ocean acidification observation data, which contribute towards the Sustainable Development Goal (SDG) 14.3 and the associated SDG Indicator 14.3.1: "Average marine acidity (pH) measured at agreed suite of representative sampling stations".

---

[24] These values are based on when in the year a pixel first experiences its highest MHW category, so no pixel is counted more than once
[25] This is taken by finding the cumulative MHW days per pixel for the entire ocean and dividing that by the overall number of ocean pixels (~690 000).
[26] https://library.wmo.int/doc_num.php?explnum_id=10100
[27] Le Quéré, C., Andrew, R. M., Friedlingstein, P., Sitch, S., Pongratz, J., Manning, A. C., et al. (2018). Global carbon budget 2017. Earth Syst. Sci. Data 10, 405–448. doi: 10.5194/essd-10-405-2018

The data are summarised in Figure 8 (left) and show an increase of variability (minimum and maximum pH values are highlighted) and a decline in average pH at the available observing sites between 2015 and 2019. The more steady global change (Figure 8, right) estimated from a wider variety of sources including measurements of other variables, contrasts with the regional and seasonal variations in ocean carbonate chemistry seen at individual sites. The increasing number of available data highlight the variability and the trend in ocean acidification and the need for sustained long-term observations to better characterize the natural variability in ocean carbonate chemistry.
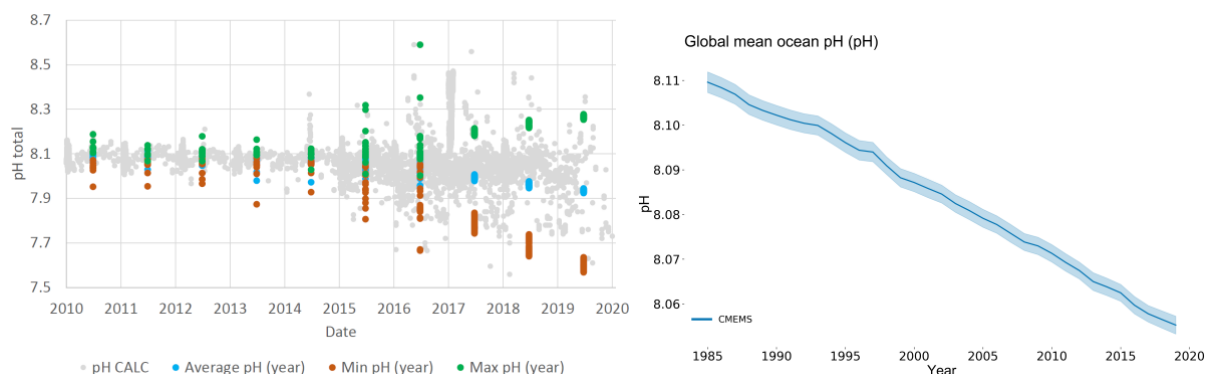

Figure 8: (left) Surface pH values based on ocean acidification data submitted to the 14.3.1 data portal (http://oa.iode.org) for the time period from 1 January 2010 to 8 January 2020. Grey circles – calculated pH of data submissions (including all data sets with data for at least two carbonate parameters); blue circles – average annual pH (based on data sets with data for at least two carbonate parameters); red circles – annual minimum pH; green circles – annual maximum pH. Note that the number of stations is not constant with time. (right) Global mean surface pH from E.U. Copernicus Marine Service Information (blue). The shaded area indicates the estimated uncertainty in each estimate.

Cryosphere

The cryosphere is the domain that comprises the frozen parts of the earth. The cryosphere provides key indicators of the changing climate, but it is one of the most under-sampled domains. The major cryosphere indicators used in the provisional statement are sea-ice extent and mass balance of the Greenland ice sheets, both of which can be routinely measured using satellite data. Specific snow events are covered in the section on **High-impact events in 2020**. Other cryosphere indicators including glacier mass balance and permafrost, which are measured *in situ,* are not covered in the provisional statement as it takes time to gather and process the data.

Sea ice

In the Arctic, the annual minimum sea-ice extent in September was the second lowest on record (Figure 9) and record low sea-ice extents were observed in the months of July and October. April and August extents were among the five lowest in the 42-year satellite data record. Antarctic sea ice remained close to the long-term average. For more details on the datasets used see **Sea ice data**.

In the Arctic, the maximum sea-ice extent for the year was reached on 5 March 2020. At just above 15 million km^2, this was the 10th or 11th (depending on the data set used) lowest maximum extent on record[28]. Sea-ice retreat in late March was mostly in the Bering Sea. In April, the rate of decline was similar to that of recent years, and the mean sea-ice extent for April was between 2nd and 4th lowest, effectively tied with 2016, 2017, and 2018.

Record high temperatures north of the Arctic Circle in Siberia (see **Sidebar: The Arctic in 2020**) triggered an acceleration of sea-ice melt in the East Siberian and Laptev Seas, which continued well

---

[28] http://nsidc.org/arcticseaicenews/2020/03/

into July. Sea-ice extent for July was the lowest on record[29] (7.28 million km^2). The sea-ice retreat in the Laptev Sea was the earliest observed in the satellite era. Towards the end of July, a cyclone entered the Beaufort Sea and spread the sea-ice out, temporarily slowing the decrease of the ice extent. In mid-August, the area affected by the cyclone melted rapidly which, combined with the sustained melt in the East Siberian and Laptev Seas, made the August extent the 2nd or 3rd lowest on record.

The 2020 Arctic sea-ice extent minimum was observed on 15 September at 3.74 million km^2, marking only the second time on record that the Arctic sea-ice extent shrank to less than 4 million km^2. Only 2012 had a lower minimum extent at 3.39 million km^2. Vast areas of open ocean were observed in the Chukchi, East Siberian, Laptev, and Beaufort Seas, notwithstanding a tongue of multi-year ice that survived the 2020 melt season in the Beaufort Sea[30] (Figure 10).

Refreeze was slow in late September and October in the Laptev and East Siberian Seas, probably due to the accumulated heat in the upper ocean since the early retreat in late June. Arctic sea-ice extent was the lowest on record for October.

In the Antarctic, the minimum sea-ice extent was observed later than usual, on 2 March, at 2.73 million km^2. Sea-ice extent was close to the climatological average for most of the year and was above average in September and October. The maximum extent was reached on 28 September at 18.95 million km^2.
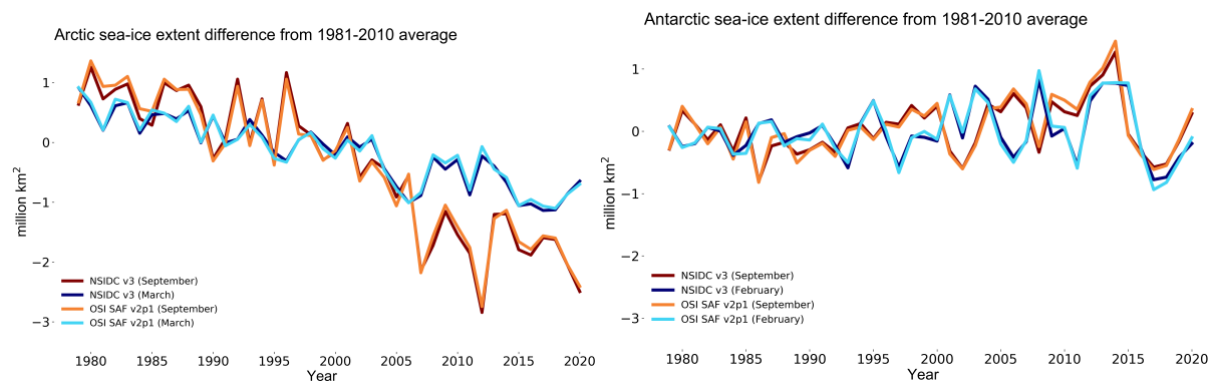
Figure 9: Sea-ice extent difference from the 1981-2010 average in the Arctic (left) and Antarctic (right) for the months with maximum ice cover (Arctic: March, Antarctic: September) and minimum ice cover (Arctic: September, Antarctic: February). Data from EUMETSAT OSI SAF v2p1 (Lavergne et al., 2019) and NSIDC v3 (Fetterer et al., 2017).

[29] https://cryo.met.no/en/arctic-seaice-summer-2020
[30] https://cryo.met.no/en/arctic-seaice-september-2020
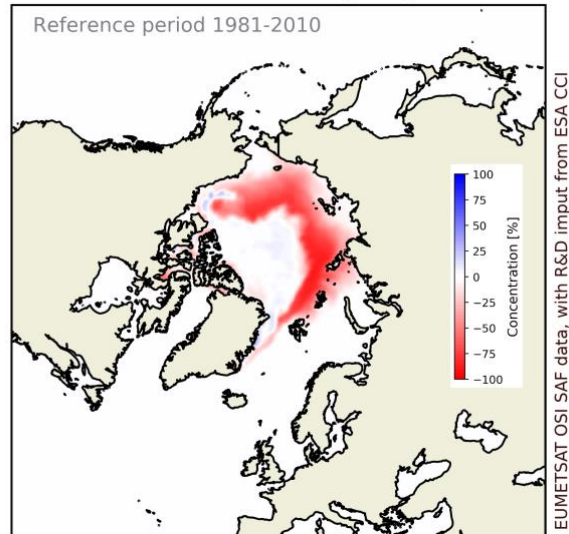
Sea Ice Concentration Anomaly, September 2020

Figure 10: Sea Ice Concentration anomaly against the 1981-2010 period for the Arctic (EUMETSAT OSI SAF v2p1 data, with R&D input from ESA CCI). Sea-ice concentration is a parameter used to describe how densely the sea ice is packed. It is expressed by a continuous scale from complete ice cover (100%) to an open ocean with no ice (0%).

Greenland Ice Sheet

Despite the exceptional warmth in large parts of the Arctic, in particular the very unusual temperatures that were observed in eastern Siberia since February 2020, temperatures over Greenland were close to the long-term mean (see Figure 2). The ice sheet ended the September 2019 to August 2020 season with an overall loss of 152 Gt (gigatons) of ice from surface melting, the discharge of icebergs and from melting of glacier tongues by warm ocean water (Figure 11). This means that the ice sheet continued to lose ice, though at a slower rate than seen in 2019 (which saw a loss of 329 Gt).

Changes in the mass of the Greenland ice sheet reflect the combined effects of surface mass balance (SMB) – defined as the difference between snowfall and run-off from the ice sheet, which is always positive at the end of the year – and mass losses at the periphery from the calving of icebergs and the melting of glacier tongues that meet the ocean. The 2019-20 Greenland SMB was +349 Gt of ice, which is close to the 40-year average of +341 Gt. However, ice loss due to iceberg calving was at the high end of the 40-year satellite record. The Greenland SMB record is now four decades long and, although it varies from one year to another, there has been an overall decline in the average SMB over time (Figure 11). In the 1980s and 1990s, the average SMB gain was about +416 Gt/year. It fell to +270 Gt in the 2000s and +260 Gt in the 2010s.

The GRACE satellites and the follow-up mission GRACE-FO measure the tiny change of the gravitational force due to changes in the amount of ice. This gives us an independent measure of the total mass balance. Based on this data, it can be seen that the Greenland ice sheet has lost about 4200 Gt from April 2002 to August 2019, which contributed to a sea level rise of slightly more than 1 cm. This is in good agreement with the mass balance from SMB and discharge, which during the same period was 4261 Gt.

The 2019-20 melt season on the ice sheet started on 22 June, 10 days later than the 1981-2020 average. As in previous years, there were losses along the Greenlandic west coast and gains in the east. In mid-August, unusually large storms brought four times the normal monthly precipitation to western Greenland, most of which fell as snow that temporarily stopped the net loss of ice and was

decisive in reducing the amount of melt, quite different from the previous year 2018-19 with extended high pressure periods and large amounts of sunshine which significantly increased the amount of melt in summer.
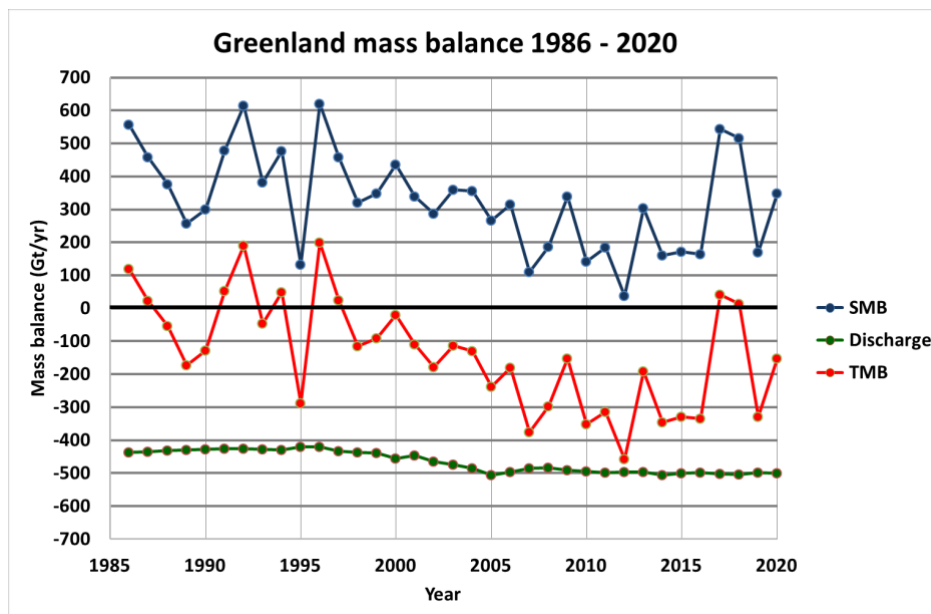

Figure 11: Components of the total mass balance of the Greenland Ice Sheet 1986-2020. Blue: Surface mass balance[31], green: discharge, red: total mass balance, the sum of Surface Mass Balance and discharge[32].

Drivers of short-term climate variability

There are many different natural phenomena, often referred to as climate patterns or climate modes, that affect weather at timescales ranging from days to several months. Surface temperatures change relatively slowly over the ocean, so recurring patterns in sea surface temperature can be used to understand and, in some cases, predict the more rapidly changing patterns of weather over land on seasonal time scales. Similarly, albeit at a faster rate, known pressure changes in the atmosphere can help explain certain regional weather patterns.

In 2020, the El Niño–Southern Oscillation, a phenomenon measured by both the oceans and the atmosphere, and the Arctic Oscillation, an atmospheric phenomenon, each contributed to specific weather events in different parts of the world. The Indian Ocean Dipole, which played a key role in the events of 2019 was near-neutral for much of 2020.

El Niño Southern Oscillation (ENSO)

ENSO is one of the most important drivers of year-to-year variability in weather patterns around the world. It is linked to hazards such as heavy rains, floods, and drought. El Niño, characterised by higher-than-average sea surface temperatures in the eastern Pacific and a weakening of the trade winds, typically has a warming influence on global temperatures. La Niña, which is characterised by below-average sea-surface temperatures in the central and eastern Pacific and a strengthening of the trade winds, has the opposite effect.

Sea-surface temperatures at the end of 2019 were close to or exceeded El Niño thresholds in the Niño 3.4 region[33]. These persisted into the early months of 2020, but the event did not strengthen

---

[31] http://polarportal.dk/en/greenland/surface-conditions/.
[32] Mankoff, K.D. et al. (2020) Greenland Ice Sheet solid ice discharge from 1986 through March 2020 Earth Syst. Sci. Data, 12, 1367–1383, https://doi.org/10.5194/essd-12-1367-2020
[33] https://origin.cpc.ncep.noaa.gov/products/analysis_monitoring/ensostuff/ONI_v5.php

and sea surface temperature anomalies in the eastern Pacific fell in March. After a six-month period of neutral conditions – that is, sea surface temperatures within 0.5 °C of normal – the cool-phase, La Niña, developed in August and strengthened in October, although it was technically still defined as weak (0.5–1.0°C below normal). The atmosphere also responded with stronger than average trade winds, indicating a coupling with the sea surface temperatures. La Niña conditions are associated with above-average hurricane activity in the North Atlantic, which has experienced a record number of named tropical storms during its 2020 hurricane season. La Niña is expected to persist through the first quarter of 2021[34].

Arctic Oscillation (AO)

The AO is a large-scale atmospheric pattern that influences weather throughout the Northern Hemisphere. The positive phase is characterised by lower-than-average air pressure over the Arctic and higher-than-average pressure over the northern Pacific and Atlantic Oceans. The jet stream is parallel to the lines of latitude and farther north than average, locking up cold Arctic air, and storms can be shifted northward of their usual paths. The mid-latitudes of North America, Europe, Siberia, and East Asia generally see fewer cold air outbreaks than usual during the positive phase of the AO. A negative AO has the opposite effect, associated with a more meandering jet stream and cold air spilling south into the mid-latitudes.

The AO was strongly positive during the Northern Hemisphere 2019-20 winter and was the strongest in February since January 1993. This contributed to the warmest winter on record for Asia and Europe and the sixth warmest for the contiguous United States, contrasted by Alaska's coldest winter in more than two decades. Additionally, the positive winter phase of the Arctic Oscillation has been linked to low sea ice extent the following summer (Rigor et al. 2002[35]). See the section on **Sea ice**.

Sidebar: The Arctic in 2020

The Arctic is undergoing drastic changes as the global temperature increases. Since the mid-1980s, Arctic surface air temperatures have warmed at least twice as fast as the global average, while sea ice, the Greenland ice sheet and glaciers have declined over the same period and permafrost temperatures have increased. This has potentially large implications not only for Arctic ecosystems, but also for the global climate through various feedbacks[36].

For the first 10 months of 2020, the Arctic stands out as the region with the largest temperature deviations from the long-term average. Contrasting conditions of ice, heat and wildfires were seen in the eastern and western Arctic (Figure 12). A strongly positive phase of the Arctic Oscillation during Winter 2019-20 set the scene early in the year, with higher than average temperatures across Europe and Asia and well-below average temperatures in Alaska, a pattern which persisted through much of the year.

In a large region of the Siberian Arctic, temperature anomalies for January to October were more than 3 °C, and in its central coastal parts more than 5 °C, above average (Figure 14). A preliminary record temperature was set for north of the Arctic Circle, of 38 °C on 20 June in Verkhoyansk[37],

---

[34] https://ane4bf-datap1.s3-eu-west-1.amazonaws.com/wmocms/s3fs-public/ckeditor/files/El-Nino-La-Nina-Update-October-2020-en.pdf?UGaW3HcT_wYatEuK8tCOdCqjq4Qr4kSb

[35] Rigor, I. G., Wallace, J. M., & Colony, R. L. (2002). Response of sea ice to the Arctic Oscillation. Journal of Climate, 15(18), 2648–2663. https://doi.org/10.1175/1520-0442(2002)015<2648:ROSITT>2.0.CO;2

[36] IPCC, 2019: IPCC Special Report on the Ocean and Cryosphere in a Changing Climate [H.-O. Pörtner, D.C. Roberts, V. Masson-Delmotte, P. Zhai, M. Tignor, E. Poloczanska, K. Mintenbeck, A. Alegría, M. Nicolai, A. Okem, J. Petzold, B. Rama, N.M. Weyer (eds.)].

[37] https://public.wmo.int/en/media/news/reported-new-record-temperature-of-38%C2%B0c-north-of-arctic-circle

during a prolonged heatwave. Heatwaves and heat records were also observed in other parts of the Arctic (see **High-impact events in 2020**) and extreme heat was not confined to the land only. An "extreme" marine heatwave affected large areas of the Arctic Ocean north of Eurasia (see Figure 7). Sea ice in the Laptev Sea, offshore from the area of highest temperature anomalies on land, was unusually low through the summer and autumn. Indeed, sea ice extent was particularly low along the Siberian coastline, with the Northern Sea Route ice-free or close to ice free from July to October.

Although the Arctic was predominantly warmer than average for this period, some regions, including parts of Alaska and Greenland, saw close-to or below-average temperatures. As a result, the 2019-20 surface mass balance for Greenland was close to the 40-year average. Nevertheless, the decline of the Greenland ice sheet continued during the 2019-20 season, but the loss was below the typical amounts seen during the last decade (see **Cryosphere**). Sea ice conditions along the Canadian archipelago were close to average at the September minimum and the western passage remained closed[38].

The wildfire season in the Arctic during 2020 has been particularly active, but with large regional differences. The region north of the Arctic circle saw the most active wildfire season in an 18-year data record, as estimated in terms of fire radiative power and CO_2 emissions released from fires. The main activity was concentrated in the eastern Siberian Arctic, which was also drier than average. Regional reports[39] for eastern Siberia indicate that the forest fire season started earlier than average, and for some regions ended later, resulting in long-term damage to local ecosystems. Alaska, as well as Yukon and the Northwest Territories reported fire activity that was well below average.

---

[38] Arctic Climate Forum https://arctic-rcc.org/sites/arctic-rcc.org/files/presentations/acf-fall-2020/2%20-%20Day%202%20-%20ACF-6_Arctic_summary_MJJAS_2020_v2.pdf
[39] https://arctic-rcc.org/sites/arctic-rcc.org/files/presentations/acf-fall-2020/3%20-%20Day%201-%20ACF%20October%202020%20Regional%20Overview%20Summary%20with%20extremes%20-281020.pdf
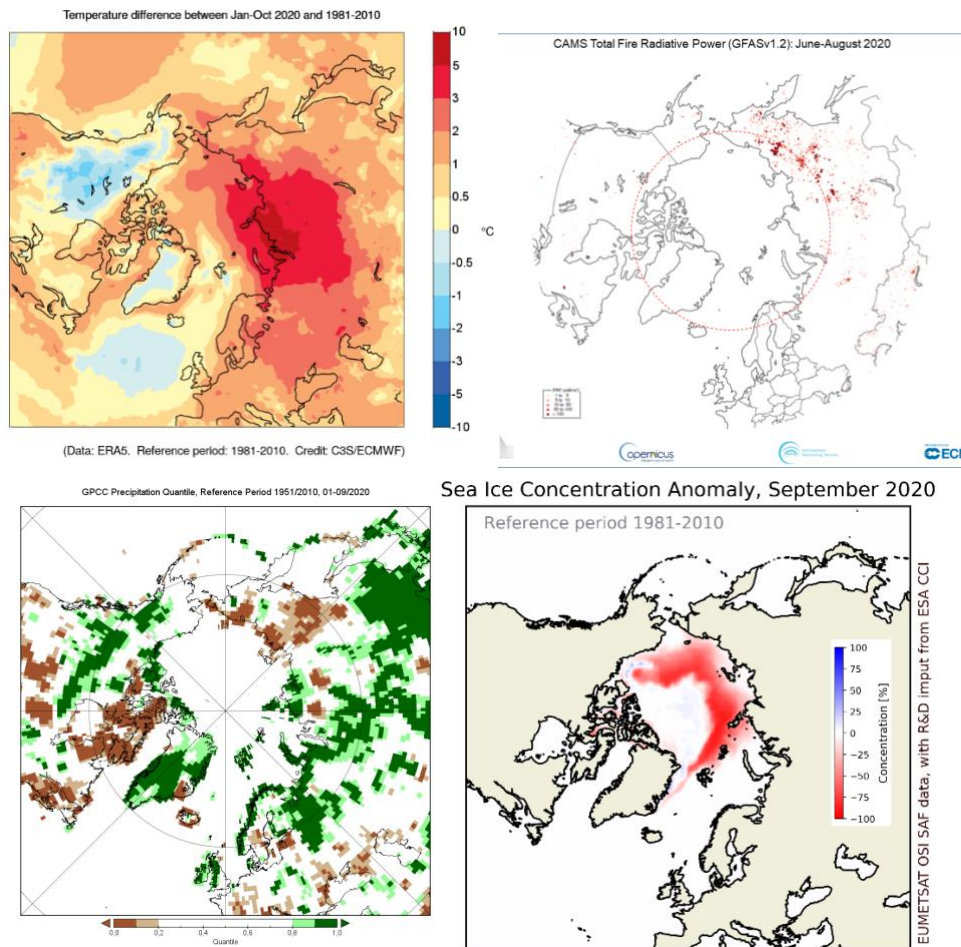
Figure 12: (top left) Temperature anomalies for the Arctic relative to the 1981-2010 long-term average from the ERA5 reanalysis for January to October 2020. Credit: Copernicus Climate Change Service, ECMWF. (top right) Fire Radiative Power, a measure of heat output from wildfires, in the Arctic Circle between June and August 2020. Credit: Copernicus Atmosphere Monitoring Service, ECMWF (bottom left) Total precipitation in Jan-Sep 2020, expressed as a percentile of the 1951–2010 reference period, for areas that would have been in the driest 20% (brown) and wettest 20% (green) of years during the reference period, with darker shades of brown and green indicating the driest and wettest 10%, respectively Credit: Global Precipitation Climatology Centre (GPCC). (bottom right) sea-ice concentration anomaly for September 2020. Credit: EUMETSAT OSI SAF data with R&D input from ESA CCI.

High-impact events in 2020

Although understanding broad-scale changes in the climate is important, the most acute impacts of weather and climate are often felt during extreme meteorological events such as heavy rain and snow, droughts, heatwaves, cold waves, and storms, including tropical storms. These can lead to or exacerbate other high-impact events such as flooding, landslides, wildfires and avalanches.

A year of widespread flooding, especially in Africa and Asia

Very extensive flooding occurred over large parts of Africa in 2020. Rainfall was well above average in most of the Greater Horn of Africa during the March-May "long rains" season, following a similarly wet season in October-December 2019. This was followed by above-average rainfall across the vast majority of the Sahel region, from Senegal to Sudan, during the summer monsoon (Figure 13). Flooding was extensive across many parts of the region, although Sudan and Kenya were the worst-affected with 285 deaths reported in Kenya[40], and 155 deaths and over 800,000 people affected in

---

[40] EM-DAT.

Sudan[41], along with further indirect impacts from disease. Countries reporting loss of life or significant displacement of populations included Sudan, South Sudan, Ethiopia, Somalia, Kenya, Uganda, Chad, Nigeria, Niger, Benin, Togo, Senegal, Côte d'Ivoire, Cameroon and Burkina Faso. Many lakes and rivers reached record high levels, including Lake Victoria in May, and the Niger River at Niamey and the Blue Nile at Khartoum in September.
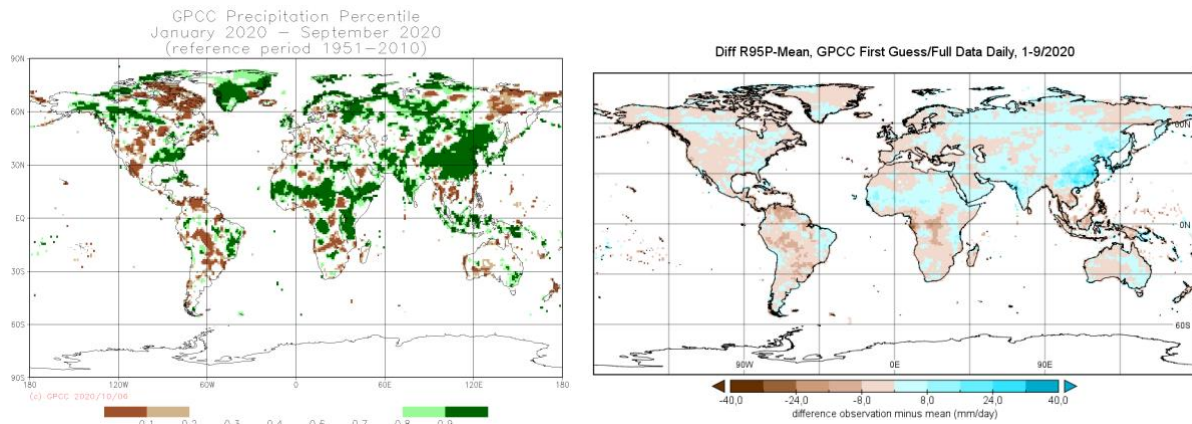

Figure 13: (left) Total precipitation in Jan-Sep 2020, expressed as a percentile of the 1951–2010 reference period, for areas that would have been in the driest 20% (brown) and wettest 20% (green) of years during the reference period, with darker shades of brown and green indicating the driest and wettest 10%, respectively (Source: Global Precipitation Climatology Centre (GPCC), Deutscher Wetterdienst, Germany). (right) Difference between the observed 95th percentile of daily precipitation total in Jan-Sep 2020 and the long-term mean based on 1982-2016 (full year). Blue indicate more extreme daily precipitation events and brown less than the long-term means.

India had one of its two wettest monsoon seasons since 1994, with nationally-averaged rainfall for June to September 9% above the long-term average. Heavy rain, flooding and landslides also affected surrounding countries. August was the wettest month on record for Pakistan, and 231 mm of rain fell on 28 August at Karachi-Faisal, the highest daily total on record in the Karachi area. More than 2000 deaths were reported during the season in India, Pakistan, Nepal, Bangladesh, Afghanistan and Myanmar[42], including 145 deaths in flash flooding in Afghanistan in late August, and 166 deaths in a landslide at a mine in Myanmar in early July, following heavy rain.

Persistent high rainfall in the Yangtze River catchment in China in the monsoon season also caused severe flooding. The June-July period was particularly wet and floods affected the Yangtze and its tributaries, with the Three Gorges Dam discharging water at its maximum capacity. Reported economic losses exceeded US$15 billion, and at least 279 deaths were reported during the period. It was also a very wet summer monsoon season over the Korean Peninsula, with the Republic of Korea experiencing its third-wettest summer, and parts of western Japan were affected by significant flooding in July.

Parts of southeast Asia experienced severe flooding in October and November. The worst affected area was central Vietnam, where heavy rains typical of the arrival of the northeast monsoon were exacerbated by a succession of tropical cyclones and depressions, with eight making landfall in less than five weeks. Hué received over 1800 mm of rain in the week from 7 to 13 October, and a total of 2615 mm for the month of October. The flooding also extended further west into Cambodia.

Other regions to experience significant loss of life in floods (mostly flash floods associated with extreme local rainfall) included Indonesia in January, Brazil in January and March, the Democratic

---

[41] Reliefweb, Situation Report, Sudan, 13 November 2020.
[42] EM-DAT.

Republic of the Congo and Rwanda in April and May, and Yemen in July. Jakarta had its wettest day since 1996 with 377 mm at Halim Airport on 1 January, and Belo Horizonte its wettest day on record with 172 mm on 24 January. Khombole in Senegal had its wettest day on record with 225.8 mm on 5 September.

Heatwaves, drought and wildfire

Severe drought affected many parts of interior South America in 2020, with the worst-affected areas being northern Argentina, Paraguay and western border areas of Brazil. It was the second-driest January-August period on record for the northeast region of Argentina, whilst rainfall for the period was also far below average in Paraguay. Estimated agricultural losses were near US$3 billion in Brazil with additional losses in Argentina, Uruguay and Paraguay. Peru also experienced drought conditions between January and March, mainly in the north of the country[43]. As the drought continued, a major heatwave stretched across the region in late September and early October, extending east and north to cover much of interior Brazil. It reached 44.6 °C on 5 October at Nova Maringá and Água Clara, whilst individual locations which had their hottest day on record included Cuiaba, Curitiba, Belo Horizonte and Asuncion. There was significant wildfire activity across all three countries from mid-year onwards, with some of the most significant wildfires occurring in the Pantanal wetlands in western Brazil.

2020 has been an exceptionally warm year in most of Russia, especially Siberia. Temperatures averaged over Russia for January to August were 3.7 °C above average, 1.5 °C above the previous record set in 2007. In parts of northern Siberia the year to date has been 5 °C or more above average. The heat culminated in late June, when it reached 38.0 °C at Verkhoyansk on the 20th, provisionally the highest known temperature anywhere north of the Arctic Circle. Abnormal warmth also extended to other parts of the high Arctic outside Russia, with temperatures reaching records on 25 July of 21.9 °C at Eureka (Canada), and 21.7 °C at Svalbard Airport. Extensive wildfires occurred through many parts of northern Siberia, contributing to record high wildfire-related carbon emissions during the Arctic summer[44], and the warmth contributed to exceptionally early sea ice retreat along the Russian Arctic coast.

A number of exceptionally large wildfires, including the largest fires ever recorded in the states of California and Colorado, occurred in the western United States in late summer and autumn. Widespread drought conditions through the western half of the country, particularly the interior southwest, contributed to the fires, as did a very weak summer monsoon. July to September were the hottest and driest on record for the southwest. Abnormal lightning activity in coastal California in mid-August also ignited many fires. The most destructive fires were in California and western Oregon, with over 8,500 structures destroyed in California and 2,000 in Oregon; 41 deaths in total were attributed to the fires across multiple states[45]. There were also a number of episodes of extreme heat. Death Valley reached 54.4 °C on 16 August, the highest known temperature in the world in at least the last 80 years, whilst 49.4 °C on 6 September at Woodland Hills was a record for greater Los Angeles.

Major wildfires in eastern Australia which had burned through the later part of 2019 continued into early 2020, before finally being controlled after heavy rain in early February. Drought conditions which had prevailed since early 2017 eased from January onwards, but there were a number of episodes of extreme heat in early 2020. Penrith in western Sydney reached 48.9 °C on 4 January, the

---

[43] https://cdn.www.gob.pe/uploads/document/file/1325635/INFORME-LLUVIAS-2019-2020%20FINAL-29-09-2020v2.pdf
[44] Copernicus Atmosphere Monitoring Service.
[45] NCEI Billion-Dollar Weather and Climate Disasters. https://www.ncdc.noaa.gov/billions/events/US/2020

highest observed in an Australian metropolitan area, whilst Canberra, which set monthly records in all three summer months, reached a new high of 44.0 °C on the same day. Severe smoke pollution also affected many parts of southeastern Australia in the early part of 2020. A number of stations in New Zealand reported their longest dry spell on record between late December 2019 and late February 2020.

A major heatwave affected the Caribbean region and Mexico in April. Temperatures reached 39.7 °C at Veguitas on 12 April, a national record for Cuba, whilst Havana also had its hottest day with 38.5 °C. In eastern Mexico temperatures exceeded 45 °C at a number of locations, reaching as high as 48.8 °C at Gallinas on 12 April, whilst very high readings in Central America included 41.2 °C at San Agustin Acasaguatlan (Guatemala). Further extreme heat in September saw national or territorial records set for Dominica, Grenada and Puerto Rico.

Dry conditions affected parts of north-central Europe during spring and summer 2020, although generally not to the same extent as in 2018 or 2019. April was especially dry, with Romania and Belarus having their driest April on record and Germany and the Czech Republic their second driest, while Geneva, Switzerland had a record 43-day dry spell from 13 March to 24 April. There was also a significant heatwave in western Europe in August. Whilst it was generally not as intense as those of 2019 (except locally on the northern coast of France), many locations, particularly in northern France, reached temperatures which ranked second behind the 2019 heatwaves, and De Bilt (Netherlands) had a record eight consecutive days above 30 °C. In early September the focus of extreme heat shifted to the eastern Mediterranean, with all-time records at locations including Jerusalem (42.7 °C) and Eilat (48.9 °C) on 4 September, following a late July heatwave in the Middle East in which Kuwait Airport reached 52.1 °C and Baghdad 51.8 °C.

It was a very hot summer in parts of east Asia. Hamamatsu (41.1 °C) equalled Japan's national record on 17 August, and Taipei had its hottest day on record with 39.7 °C on 24 July. Hong Kong had a record run of 13 consecutive hot nights, with a daily minimum temperature of 28 °C or above, from 19 June to 1 July, followed by 11 consecutive hot nights from 5 to 15 July.

Long-term drought continued to persist in parts of southern Africa, particularly the Northern and Eastern Cape Provinces of South Africa, although heavy winter rains saw water storages reach full capacity in Cape Town, continuing the recovery from extreme drought, which peaked in 2018. Rainfall during the 2019-20 summer rainy season in interior southern Africa was locally heavy, but long-term drought persisted in some areas.

Extreme cold and snow

North America's most significant snowstorm of the 2019-20 winter occurred on 17-18 January in Newfoundland. St. John's received 75 cm of snow, including a record daily snowfall, and wind gusts of 126 km/h. Later in the year, there were two extreme early-season cold episodes in autumn. In the second week of September, widespread snowfalls occurred in lowland Colorado, including Denver, where a September record high of 38.3 °C had been set only three days earlier, on 5 September. Later, in October, a major cold outbreak brought exceptionally low temperatures and winter precipitation across a broad region of the Rocky Mountains and central states. A damaging ice storm in Oklahoma City saw power outages which lasted for days across more than half the city, whilst further north, Potomac, Montana reached −33.9 °C on 25 October, the earliest autumn date on which temperatures had fallen below −30 °C at a climate station anywhere in the United States (excluding Alaska).

The extremely wet and warm winter in northern Europe resulted in exceptionally low snow cover in many places – Helsinki experienced a record low number of snow-covered days, breaking the previous record by a wide margin – but in far northern Europe, where temperatures were above average but still cold enough for snow, the snowpack was exceptionally heavy. At Sodankylä (Finland), the snowpack reached record depths in mid-April. A cold May led to a delayed melt with some cover persisting into June, while flooding occurred in late May and early June with the spring melt. Rain-on-snow events prevented some reindeer herds from reaching feed.

It was a cold winter in southern South America. Tierra del Fuego had its most significant cold spell since 1995 in late June and early July, with Rio Grande recording a maximum of −8.8 °C and minimum of −16.5 °C on 1 July. Paraguay saw record minimum temperatures for August in a number of places. Snow cover in Patagonia was the second-most extensive since 2000 and sea ice formed along parts of the Tierra del Fuego coast. Some stock losses were reported. In August, a cold wave in the north of Peru's Amazonia saw temperatures at Caballacocha reach 12.8°C, the lowest temperature recorded there since 1975.

Abnormal low-elevation snowfalls occurred in Tasmania in early August. On 4 August, snow settled to sea level in Launceston, the city's most significant snowfall since 1921. Liawenee, in the central highlands, reached −14.2 °C on 7 August, a Tasmanian record low.

Tropical storms and an exceptionally active North Atlantic hurricane season

The number of tropical cyclones globally was above average in 2020, with 96 named tropical storms (to 17 November) in the 2020 Northern Hemisphere and 2019-20 Southern Hemisphere seasons. The North Atlantic region had a very active season, with 30 tropical cyclones as of 17 November, more than double the long-term average and breaking the record for a full season, set in 2005. Most other basins had cyclone numbers near or slightly below average.

The Accumulated Cyclone Energy (ACE) index, which integrates cyclone intensity and longevity, was well below average in all basins except the North Atlantic and North Indian Oceans, with the Northwest Pacific about 50% below the long-term average. Whilst ACE seasonal values for the North Atlantic were above average, they were well short of seasonal records.

The exceptionally active North Atlantic season resulted in a large number of landfalls. 12 systems made landfall in the United States, breaking the previous record of nine; five of them in the state of Louisiana. The most severe impacts of the season in the United States came from Laura, which reached category 4 intensity and made landfall on 27 August near Lake Charles in western Louisiana, with extensive wind and storm surge damage. Laura was also associated with extensive flood damage in Haiti and the Dominican Republic in its developing phase. 77 deaths and US$14 billion in economic losses[46] were attributed to the storm across the three countries. Later in the season, two major hurricanes made landfall in rapid succession in Central America. Hurricane Eta made landfall as a category 4 system on the east coast of Nicaragua on 3 November, causing severe flooding in the region as it moved slowly across Nicaragua, Honduras and Guatemala. Eta moved offshore on 6 November and re-intensified to a tropical storm, making further landfalls in Cuba and on the Florida Keys. Iota was even stronger, becoming the season's first category 5 system off the Nicaraguan coast on 16 November.

---

[46] NCEI Billion-Dollar Weather and Climate Disasters (economic losses), EM-DAT (deaths).

Other damaging landfalls in the United States included those of Isaias in August in North Carolina and Sally in September in Alabama, whilst other parts of the region to experience significant damage during the season included Bermuda, the Bahamas and the Yucatan Peninsula of Mexico.

Cyclone Amphan, which made landfall on 20 May near the India-Bangladesh border in the eastern Bay of Bengal, was the costliest tropical cyclone on record for the North Indian Ocean with reported economic losses in India of approximately US$14 billion[47]. Large-scale evacuations of coastal areas in India and Bangladesh meant that casualties were far lower than in previous comparable cyclones in the region. Nevertheless, 129 lives were lost across the two countries. Amphan reached category 5 equivalent intensity whilst over the Bay of Bengal and, whilst it weakened somewhat before landfall as a category 2 storm, it still led to extensive wind and storm surge damage in the city of Kolkata and surrounds.

Harold, in the Southwest Pacific in April was another category 5 cyclone. Its most significant impacts were in the northern islands of Vanuatu, where it made landfall at near peak intensity on 6 April. More than 17 000 homes were damaged or destroyed[48], and about 65% of Vanuatu's population was affected[49], with the city of Luganville amongst the hardest hit. There was also significant damage in Fiji as Harold passed to the south of the main island of Viti Levu, whilst damage also occurred in Tonga and the Solomon Islands. 30 deaths were reported along the cyclone's path, most of them when high seas washed passengers overboard from a ferry in the Solomon Islands.

The strongest tropical cyclone of the season was Typhoon Goni (Rolly)[50]. It crossed the northern Philippines on 1 November with a 10-minute mean wind speed of 220 km/h (or higher) at its initial landfall, making it one of the most intense landfalls on record. This was followed the next week by Vamco (Ulysses), which was less intense but caused severe flooding in Manila and other areas. At least 25 deaths were attributed to Goni (Rolly) and 67 to Vamco (Ulysses)[51]. Two major tropical cyclones hit the Korean Peninsula within a few days in early September, with Typhoon Mayask (Julian) making landfall near Busan on 3 September, followed by Haishen (Kristine) on the 7th. Mayask (Julian) brought 963.5mm of rainfall over two days to a site on Jeju Island, and wind gusts on the island up to 177 km/h. Both tropical cyclones led to significant flooding on the Korean Peninsula and in western Japan, and 41 lives were lost when a ship sank off western Japan during the passage of Maysak. Eight tropical cyclones and depressions made landfall in Vietnam in less than five weeks in October and November, contributing to major flooding in the region (see Floods section).

Other tropical cyclones associated with significant loss of life through flooding were Cyclone Diane in Madagascar in January, and Tropical Storm Amanda in Guatemala and El Salvador in May.

Extratropical cyclones and severe local storms

One of the costliest extreme events of the year was a derecho (fast-moving line of severe thunderstorms) which moved across the U.S. Midwest on 10 August, extending from South Dakota to Ohio. Iowa was the worst-affected area, with severe agricultural losses, including an estimated 2 million hectares of corn and soybean crops flattened. Over 90% of the buildings in the city of Cedar Rapids were damaged. Total losses were estimated at US$7.5 billion. The U.S. tornado season to date has been near average, with the two most significant outbreaks affecting the Nashville area on 2-3 March and a broad area extending from Texas to Maryland on 12-13 April. 25 lives were lost in

---

[47] EM-DAT
[48] Australian Department of Foreign Affairs and Trade, https://www.dfat.gov.au/crisis-hub/Pages/tropical-cyclone-harold.
[49] FAO, http://www.fao.org/resilience/resources/resources-detail/en/c/1274007/
[50] Names in parentheses are alternative local names for the storms
[51] Philippines National Disaster Risk Reduction and Management Council, situational reports.

the March outbreak and 35 in the April outbreak, with losses of several billion dollars across the two events[52].

Severe thunderstorms affected a wide area of eastern Australia in the third week of January. The most significant damage was in Canberra, where hail five cm in diameter on 20 January led to extensive vehicle and building damage across a broad swathe of the city. Significant hail damage also occurred in some eastern suburbs of Melbourne. Total losses from the storms were estimated at US$1.1 billion[53]. Further major hailstorms affected Queensland on 31 October with hailstones as large as 14 cm in diameter reported in the suburbs of Brisbane. Other major severe storms included a squall line which crossed southern Brazil on 30 June, with tornadoes, hail and wind gusts exceeding 100 km/h, with 12 deaths reported, and a hailstorm in Tripoli (Libya) on 27 October with hailstones as large as 20 cm.

A number of severe extratropical cyclones affected northern, central and western Europe in February, contributing to a very wet month with flooding in some areas[54]. The most significant storm of this period was Ciara (also known as Sabine and Elsa), which passed to the northwest of Europe on 10-11 February. Significant wind damage extended from Ireland to Sweden, Poland and Italy. In the autumn, Storm Alex in early October brought extreme winds to western France with gusts as high as 186 km/h, whilst heavy rain extended across a wide area. 3 October was the wettest area-averaged day on record for the United Kingdom with a national average of 31.7 mm, whilst extreme rainfall occurred near the Mediterranean coast on both sides of the France-Italy border, with 24-hour totals exceeding 600 mm in Italy and 500 mm in France. The extreme rainfall extended to southern Switzerland with 421 mm in 24 hours at Càmedo. Significant flash flooding occurred in all three countries.

A Mediterranean cyclone hybrid system ('Medicane'), showing some characteristics of a tropical cyclone and others of a mid-latitude storm, developed in mid-September, making landfall in southwestern Greece on the 18th with wind gusts exceeding 110 km/h. Earlier, it brought heavy rainfall and flash flooding to coastal Libya, with a daily rainfall total of 150.5 mm at Sabratha on 15 September.

Sidebar: Climate indicators and the sustainable development goals

The 2030 Agenda for Sustainable Development provides a shared blueprint for peace and prosperity for people and the planet, now and into the future. At its heart are a set of sustainable development goals (SDGs), which recognize that ending poverty and other deprivations must go hand-in-hand with strategies that improve health and education, reduce inequality, and spur economic growth, while tackling climate change and preserving oceans and forests. The achievement of many of these goals is put at risk by climate change, however. For example, rising temperatures are leading to the loss of species and ecosystems, which can reduce agricultural and fishing yields—contributing to food insecurity and affecting livelihoods (SDGs 1, 2, 14, & 15). Extreme weather and climate events can cause health risks, damage infrastructure and lead to water scarcity (SDGs 1, 3, 9, 11 & 6). These threats, together with others, are inter-related with conflict and stability (SDG 16). It is critical to highlight that these risks will not impact all populations or regions equally and can reinforce or worsen existing inequalities (SDG 10).

The figure below demonstrates how rising atmospheric CO_2 concentrations lead to cascading effects via six of the other key climate indicators. Beyond posing risks to achieving sustainable development,

---

[52] All impact assessments in this paragraph from NCEI Billion-Dollar Weather and Climate Disasters.
[53] Insurance Council of Australia, media release 27 August 2020.
[54] Austria contribution, Bosnia Herzegovina contribution.

some of these processes also have the potential to release further greenhouse gases into the atmosphere in a feedback loop that can perpetuate warming. For example, rising temperatures can thaw permafrost, releasing more carbon into the atmosphere.
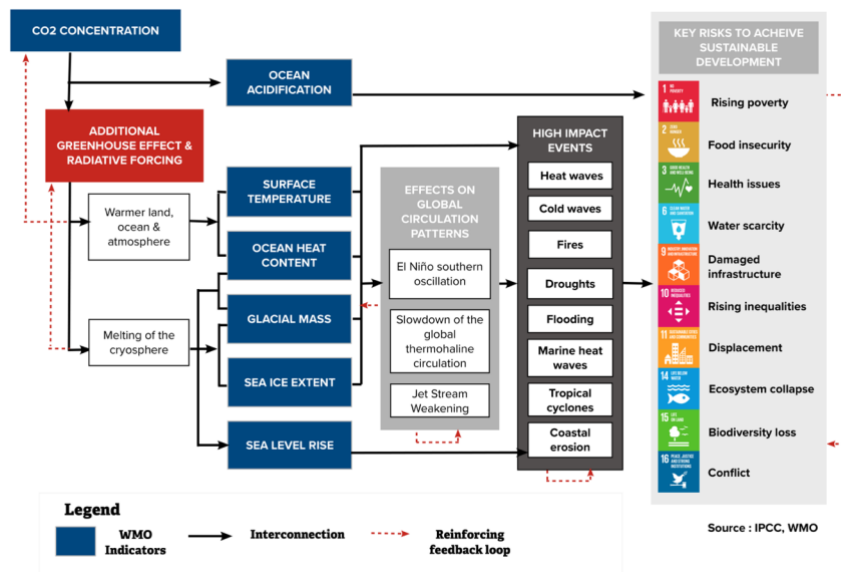

Figure 14: Selected climate change-related risks to the SDGs.

ICRC (2020). When rain turns to dust: Understanding and responding to the combined impact of armed conflicts and the climate and environment crisis on people's lives. (2020). https://www.icrc.org/sites/default/files/topic/file_plus_list/rain_turns_to_dust_climate_change_conflict.pdf

IPCC, 2014: Climate Change 2014: Synthesis Report. Contribution of Working Groups I, II and III to the Fifth Assessment Report of the Intergovernmental Panel on Climate Change [Core Writing Team, R.K. Pachauri and L.A. Meyer (eds.)]. IPCC, Geneva, Switzerland, 151 pp. https://www.ipcc.ch/report/ar5/syr/

Trewin et al.. (in press). Headline indicators for global climate monitoring. Bulletin of the American Meteorological Society. Accepted for publication. https://doi.org/10.1175/BAMS-D-19-0196.1

WMO Statement on the State of the Global Climate in 2019. (2020). World Meteorological Organization. https://library.wmo.int/doc_num.php?explnum_id=10211

United Nations (2015). "THE 17 GOALS | Department of Economic and Social Affairs." https://sdgs.un.org/goals

Sidebar: Global Climate Observing System

Climate monitoring is performed by a system of systems covering atmosphere, oceans, hydrology, the cryosphere and biosphere. Each of these areas is monitored in different ways by a range of organisations. Cutting across all these areas, satellite observations are a major contributor to global climate observations.

2016 Essential Climate Variables (ECVs)

Atmospheric

Surface

Precipitation, Surface pressure, Surface radiation budget, Surface wind speed and direction, Surface temperature, Surface water vapour

Upper-air

Earth radiation budget, Lightning, Upper-air temperature, Upper air water vapor, Upper-air wind speed and direction

Composition

Aerosols properties, Carbon dioxide, Methane and other greenhouse gases, Cloud properties, Ozone, Aerosol and ozone precursors

Oceanic

Physical

Ocean surface heat flux, Sea ice, Sea level, Sea state, Sea surface Salinity, Sea surface temperature Subsurface currents, Subsurface salinity, Subsurface temperature

Biogeochemical

Inorganic carbon, Nitrous oxide, Nutrients, Ocean colour, Oxygen, Transient tracers

Biological/ecosystems

Marine habitat properties, Plankton

Terrestrial

Hydrology

Groundwater, Lakes, River discharge, Soil moisture

Cryosphere

Glaciers, Ice sheets and ice shelves, Permafrost, Snow

Biosphere:

Above-ground biomass, Albedo, Fire, Fraction of absorbed photosynthetically active radiation, Land cover, Land surface temperature, Latent and sensible heat fluxes, Leaf area index, Soil carbon

Human use of natural resources:

Anthropogenic greenhouse gas fluxes, Anthropogenic water use

In 1992, the Global Climate Observing System (GCOS) was established by WMO, IOC, UNEP and ISC[55] to coordinate these observations and facilitate the development and improvement of global climate observations. GCOS has identified a set of variables that, when observed, should provide the necessary information to understand, model and predict the trajectory of the climate as well as plan mitigation and adaptation. The status of the observations of these variables, called Essential Climate Variables (ECV), are monitored by GCOS, which publishes regular status reports. GCOS also identifies what is needed to improve the system in Implementation reports.

GCOS works through three panels for the atmosphere, ocean and terrestrial systems. These panels are jointly sponsored with the World Climate Research Programme (WCRP), and the Global Ocean Observing System (GOOS), for the oceans.

While the GCOS networks, GSN and GUAN, provide a baseline network measuring meteorological variables, National Meteorological and Hydrological Monitoring Services (NMHS), coordinated by WMO, provide a more comprehensive and widespread network of measurements. Also, WMO's Global Atmospheric Watch (GAW) coordinates atmospheric composition measurements, ensuring reliable and accurate data, from measurements made by WMO Members, research institutions and/or agencies and other contributing networks.

Ocean observations of ocean physics, geobiochemistry biology and ecosystems are coordinated through GOOS. The Ocean Observations Physics and Climate Panel (OOPC) jointly sponsored by GCOS, GOOS and WCRP, identifies oceanic ECV and incorporates them into ocean network design. The GOOS Observations Coordination Group (OCG) monitors the performance of these networks[56] and produces an annual Ocean Observing System Report Card.

In the terrestrial domain there are a wider group of observing networks. Hydrological observations are generally operated by NMHS and coordinated through WMO. There are a number of Global Terrestrial Networks (GTN) that report to GCOS. These include the GTN-Hydrology (GTN-H) that itself is a collaboration of other networks such as those covering lakes, rivers, groundwater, soil moisture,

---

[55] World Meteorological Organization, Intergovernmental Oceanographic Commission of UNESCO, United Nations Environment Programme, and International Science Council.

[56] https://www.ocean-ops.org/

and water use. The GTN-Permafrost (GTN-P) GTN-Glaciers (GTN-G) with the World Glacier Monitoring Service (WGMS) are increasingly cooperating with the WMO Global Cryosphere Watch (GCW). GOFC-GOLD covers above-ground biomass, forests, land use and wildfires and mainly provides guidance and calibrations for the mainly satellite-based observations that are needed to cover ecosystems across the globe.

In addition to this there are a number of regionally based networks that are significant contributors to the networks: some are nationally based while others cover wider regions.

The CEOS/CGMS Joint Working Group on Climate (WGClimate) bases the development of satellite observations for climate on the ECV requirements established by GCOS. They have produced an ECV Inventory that includes records for 766 climate data records for 33 ECV covering 72 separate ECV products with more planned. Satellite observations have some advantages, they have a near-global coverage, but optical observations can be interrupted by clouds. Used with ground-based observations, either as complementary data sets, or for validation and calibration they form an invaluable part of the global observing system.

Risks and impacts

The risk of climate-related impacts depends on complex interactions between climate related hazards and the vulnerability, exposure and adaptive capacity of human and natural systems. At current levels of global greenhouse gas emissions, the world remains on course to exceed the agreed temperature thresholds of either 1.5 °C or 2 °C above pre-industrial levels, which would increase the risk of pervasive effects of climate change beyond what is already seen.

Climate-related events already pose risks to society through impacts on health, food and water security as well as human security, livelihoods, economies, infrastructure and biodiversity. Climate change also has implications for ecosystem services. It can affect patterns of natural resource use, as well as the distribution of resources across regions and within countries.

Climate change and individual events have a large environmental effect as well. Negative environmental effects include impacts on the land such as droughts, wildfires in forest and peatland areas, land degradation, sand and dust storms, and desertification. Air pollution is linked to the use of fossil fuels. In freshwater systems, floods and water stress, and in marine systems a variety of impacts including sea level rise, ocean acidification, reduced levels of ocean oxygen, mangrove decay and coral bleaching. Many of these impacts are linked to biodiversity loss. For example, besides the heavy human impacts of the wildfires in Australia in 2019 and early 2020, there were likely severe loss or displacement of many millions of animals[57] during the disaster.

Human mobility and displacement

Climate and weather events have had major and diverse impacts on population movements and on the vulnerability of people on the move throughout the year. In line with previously reported patterns, many of the largest scale displacements were in populous Asian countries. Furthermore, the complexity of human-mobility-related risk and impacts tends to be greatest - and least understood due to major limitations in the available data - in relation to slow-onset events and in fragile and conflict-affected contexts. Knowledge in this area remains relevant for global and national policy development, operations and research in the domains of human mobility and climate

---

[57]
https://www.aph.gov.au/About_Parliament/Parliamentary_Departments/Parliamentary_Library/pubs/rp/rp1920/Quick_Guides/AustralianBushfires

action. In 2020, the COVID19 pandemic has added a further dimension to human mobility concerns highlighting the need for an integrated approach to understanding and addressing climate risk and impacts on vulnerable populations.

Weather and climate-related hazards and disasters driving new displacement

Over the past decade (2010-2019), weather-related events have triggered an estimated 23.1 million displacements of people on average each year[58]. The overwhelming majority of these movements take place within national borders, though cross-border movements may also occur. Some 9.8 million displacements, largely due to hydro-meteorological hazards and disasters, were recorded during the first half of 2020, mainly concentrated in South and South-east Asia and the Horn of Africa[59]. Events in the second half of the year, including displacements linked to flooding across the Sahel region, the active Atlantic hurricane season and typhoon impacts in South-east Asia, are expected to bring the total for the year close to the average for the decade.

In May, Cyclone Amphan hit the Sundarbans region between India and Bangladesh. 2.4 million people were displaced in India, mostly in West Bengal and Odisha, and 2.5 million in Bangladesh. While many returned relatively soon afterwards, damage to more than 2.8 million homes likely resulted in homelessness and prolonged displacement for many thousands[60]. Many displaced people did not have access to evacuation centres and were compelled to take shelter in tents or in the open air on embankments[61].

Monsoon rains led to massive flooding, dam collapses, landslides, and the displacement of millions of people in Bangladesh, China, India, Japan, Pakistan[62], Nepal[63], South Korea[64], Turkey[65] and Vietnam. The floods and landslides in China were particularly intense. 29 000 homes were destroyed and over 2.2. million people evacuated by mid July 2020[66].

In July, flooding and landslides affected several districts across Nepal. IOM assessments in August showed the presence of a total of 5 467 persons from 1 066 households in 29 displacement sites across the country[67]. By September, only 12 sites were still active, hosting some 2 000 individuals in three districts, as people returned home with the end of the monsoon season[68].

In the Philippines, Super Typhoon Goni (locally known as Rolly) displaced 400,000 when it made landfall across the Philippines on 1 November[69]. Two weeks later, Typhoon Vamco triggered a further 320 000 displacements[70]. In October 2020, Cyclone Molave, the fourth storm of the month to hit Vietnam, triggered the evacuation of some 1.3 million people and left hundreds of thousands of people in a critical situation as crops were destroyed[71].

---

[58] Data sourced from the Internal Displacement Monitoring Centre's Global Internal Displacement Database (GIDD).
[59] IDMC, Internal Displacement 2020: Mid-year Update
[60] Ibid.
[61] Ibid.
[62] http://floodlist.com/asia/pakistan-glof-golen-valley-chitral-july-2020
[63] https://www.aljazeera.com/videos/2020/07/25/south-asia-monsoon-more-than-130-people-killed-in-nepal-floods/
[64] http://floodlist.com/asia/south-korea-flash-floods-july-2020
[65] http://floodlist.com/asia/turkey-rize-floods-july-2020
[66] Xinhua Net, China increases disaster relief funds amid floods, 13 July 2020
[67] https://dtm.iom.int/reports/nepal-%E2%80%93-landslides-and-floods-displacement-%E2%80%93-site-assessment-report-september-2020
[68] https://dtm.iom.int/reports/nepal-%E2%80%93-landslides-and-floods-displacement-%E2%80%93-site-assessment-round-2-october-2020
[69] https://disasterphilanthropy.org/disaster/super-typhoon-goni/, https://www.voanews.com/east-asia-pacific/aid-groups-urge-assistance-after-super-typhoon-goni-hits-philippines https://reliefweb.int/sites/reliefweb.int/files/resources/Philippines%20-%20Typhoon%20Goni%20-%20Flash%20Update%20No.%201%20(as%20of%2031%20October%202020,%209%20p.m.%20local%20time).pdf
[70] https://www.thenewhumanitarian.org/maps-and-graphics/2020/11/16/typhoon-vamco-philippines-vietnam-flooding-climate-change
[71] https://media.ifrc.org/ifrc/press-release/homes-1-million-people-ruin-major-typhoon-hits-viet-nam/

2020 also saw some of the largest wildfires on record, which led to significant displacement. The 2020 fire season in the USA resulted in the destruction of at least 2 000 residential buildings in California and displaced some 100 000 people. In Oregon around 500 000 people were placed under evacuation notice and more than 40 000 had to be evacuated from their homes[72]. In Australia, around 65 000 new displacements were recorded as a consequence of the fires that affected the country between July 2019 and February 2020. Fires also destroyed 3 100 homes, potentially leading to longer-term displacement of some 8 100 people[73].

Patterns of protracted, prolonged and repeated displacement linked with hydro-meteorological hazards

Many displacement situations triggered by hydro-meteorological events have become prolonged or protracted for people unable to return to their former homes or without options for integrating locally or settling elsewhere. While several storms and floods have led to damage in Mozambique in 2020, over a year after cyclones Kenneth and Idai hit the country in March and April 2019, tens of thousands of people remain displaced and held back from recovery[74]. An assessment conducted in October 2020 identified 93 324 people still displaced in the country's central region (of which 81 251 were displaced by Idai and 12 073 by the 2020 floods)[75]. In Cabo Delgado, almost 6 500 internally displaced people were staying in displacement sites[76].

Due to continuing or growing risk in their areas of origin (and return) or settlement, people who have been displaced by hydro-meteorological and climatic events may also be subject to repeated and frequent displacement, leaving little time for recovery between one shock and the next. This has implications for disaster preparedness and management, but also for supporting solutions to displacement that are sustainable and supporting the resilience of people who might otherwise see their living conditions progressively eroded through repeated disasters and displacement.

Compounded risk and vulnerability

Refugees, internally displaced people and migrants are often among those most vulnerable to climate and weather-related hazards. Many vulnerable people on the move, regardless of their reasons for moving, end up settling in high risk areas, where they are exposed to climate and weather hazards at a range of scales. Weather hazards and human mobility may also intersect with social and political tensions and conflict in complex settings and, as such, require the integrated consideration of multi-hazard disaster risk reduction measures, including early warning systems and preparedness, and longer-term sustainable development concerns, such as land use and urban planning.

Specific conditions of risk from hydro-meteorological disasters are particularly well documented in the Rohingya refugee sites in Cox's Bazar, Bangladesh. Over the year, a total of 162 275 have been affected, with many requiring specific assistance[77]. Without preparedness measures undertaken in the camp areas, including kits for strengthening shelters, building of retaining structures on hillsides, and improving drainage, roads and bridges, these impacts would have been worse[78].

---

[72] https://storymaps.arcgis.com/stories/064d9b11d0584625ba57b172612699c1
[73] https://www.internal-displacement.org/sites/default/files/publications/documents/Australian%20bushfires_Final.pdf
[74] UNHCR, https://www.unhcr.org/news/stories/2020/3/5e6a6e50b/year-people-displaced-cyclone-idai-struggle-rebuild.html
[75] https://displacement.iom.int/reports/mozambique-%E2%80%93-covid-19-preparedness-assessment-resettlement-sites-report-12-october-2020
[76] https://reliefweb.int/report/mozambique/rapid-response-plan-cabo-delgado-province-mozambique-may-december-2020;
https://dtm.iom.int/reports/mozambique-%E2%80%93-covid-19-preparedness-assessment-resettlement-sites-cabo-delgado-and-nampula
[77] https://www.arcgis.com/apps/MapSeries/index.html?appid=1eec7ad29df742938b6470d77c26575a
[78] UNHCR, https://www.unhcr.org/refugeebrief/the-refugee-brief-22-may-2020/

In East Africa, floods and the worst desert locust infestation in 25 years, resulted in large-scale displacement. In Somalia, floods were associated with the displacement of over one million people in 2020, mostly inside the country, while drought-related impacts induced a further 80,000 displacements[79,80]. Around a quarter of the population affected by floods this year were people already living in overcrowded and insecure camps for internally displaced people[81], to which many newly flood-displaced people also moved[82]. Farmers whose crops were devastated by desert locusts were also forced to move in search of survival assistance[83].

In Ethiopia, over 300 000 displacements were brought on by floods and landslides during the first half of the year, two thirds of which were in the Somali region[84]. IOM assessments between June and July 2020 have shown the presence of at least 104 696 people displaced by floods and of 351 062 by droughts in the country's South-East - respectively 6% and 19% of the local displaced population. Sudan experienced flash floods and rivers, including the Nile, overflowed in August. Some 125 000 refugees and internally displaced persons were among those affected[85].

Between August and September 2020, extreme rainfall triggered floods that struck several countries in the Sahel. IOM assessments estimated a total of 1.25 million people displaced in Burkina Faso, Mali and Niger - in contexts already characterized by conflict and food insecurity, as well as forced internal and cross-border population movements. The further degradation of living conditions and livelihoods resulting from the floods increased the risk of displacement within the region, southward to coastal countries and northward to North Africa and Europe[86]. Floods in August 2020 in N'Djamena, Chad, resulted in 31,853 individuals fleeing their homes and finding shelter elsewhere in the city, with little relief assistance being provided. Floods also affected the Lac province, displacing over 4,000 people, and affecting many more who had previously been displaced by conflict and violence[87].

In Yemen, where more than 80% of the total population is in need of humanitarian assistance, severe flash floods displaced many who were already internal displaced because of the conflict, living in conditions of abject poverty, in precarious shelters and without access to secure, alternative places in which to shelter. Some 300 000 people lost their homes, crops, livestock and belongings due to rain and floods. The sudden breaching of the Al-Roone dam affected thousands of people in IDP sites in Al-Tahseen, Souq al-Lill and elsewhere[88].

In Syria from early October, wildfires in Lattakia, Tartous and Homs affected up to 40 000 people through damage to housing and assets and major loss of livelihoods. Some 25 000 displacements

[79] UNHCR Somalia Factsheet, 1-30 September 2020 https://data2.unhcr.org/en/documents/details/83089
[80] Executive Committee of the High Commissioner's Programme, "Update on UNHCR's operations in the East and Horn of Africa and the Great Lakes, 29 September 2020", Seventy-first session, 5-9 October 2020, https://www.unhcr.org/5f734d884.pdf
[81] IDMC, Disasters meet political unrest, displacing millions in East Africa, July 2020 https://www.internal-displacement.org/expert-opinion/disasters-meet-political-unrest-displacing-millions-in-east-africa
[82] Executive Committee of the High Commissioner's Programme, "Update on UNHCR's operations in the East and Horn of Africa and the Great Lakes, 29 September 2020", Seventy-first session, 5-9 October 2020, https://www.unhcr.org/5f734d884.pdf and UNHCR briefing note on Somalia
[83] IDMC, Internal Displacement 2020: Mid-year Update, p.9 https://www.internal-displacement.org/publications/internal-displacement-2020-mid-year-update
[84] OCHA, Ethiopia floods response plan, Belg/Gu Season floods May 2020, 22 May 2020 https://reliefweb.int/report/ethiopia/ethiopia-floods-response-plan-belggu-season-floods-may-2020
[85] UNHCR, "Massive floods in Sudan impact thousands of refugees", 24 September 2020 https://www.unhcr.org/news/stories/2020/9/5f6c42834/massive-floods-sudan-impact-thousands-refugees.html
[86] UNHCR Sahel Crisis Response Progress Report: Responding to the urgent needs of refugees, internally displaced, returnees and others of concern, January-September 2020. https://reporting.unhcr.org/sites/default/files/UNHCR%20Sahel%20Appeal%20-%20Progress%20Report%20-%20January%20to%20September%202020%20.pdf
[87] https://dtm.iom.int/chad, https://reliefweb.int/disaster/fl-2020-000192-tcd
[88] UNHCR, "300,000 people lose homes, incomes, food supplies and belongings due to catastrophic flooding in Yemen", 21 August 2020. https://www.unhcr.org/news/briefing/2020/8/5f3e7faf4.html

were reported, including from areas with recently returned IDPs. The resilience of affected communities has been eroded over 10 years of conflict, as well as by the COVID-19 pandemic, economic crisis and the preceding massive uptake of displaced people[89].

COVID19 impacts

Mobility restrictions and economic downturns due to COVID-19 have slowed the delivery of humanitarian assistance to vulnerable people on the move as well as efforts to support recovery for affected persons, including durable solutions for those displaced. The vulnerabilities of displaced populations, who often live in densely populated settlements, were amplified further[90].

Cyclone Harold, one of the strongest storms ever recorded in the South Pacific, which struck Fiji, the Solomon Islands, Tonga and Vanuatu[91] triggered an estimated 99 500 displacements. Because of COVID-19 lockdowns and quarantines, response and recovery operations were hampered leading to delays in providing equipment and assistance[92].

Likewise, in the Philippines, the pandemic complicated evacuation and response efforts ahead of Tropical Cyclone Vongfong (Ambo) in mid-May. Over 180 000 people were pre-emptively evacuated[93], through operations were hampered by the need for social distancing measures as residents could not be transported in large numbers and evacuation centres could only be used at half capacity[94]. The storm also damaged Bicol Region's only COVID-19 testing facility[95].

In northern Central America, some 5.3 million people were in need of humanitarian assistance including 560 000 internally displaced people before the onset of the pandemic[96]. Responses to storms and cyclones that repeatedly affected the area throughout the Atlantic hurricane season have therefore taken place in a context of complex, interlinked vulnerability, linked to pre-COVID19 and COVID-19-related challenges.

Creating the conditions that enable people's options to safely stay, to leverage the full potential benefits of dignified migration, and to avert, minimise and address displacement and related protection needs is a significant concern for both climate and human mobility policies and cooperation - especially as countries are faced with decisions to expand mobility options that have been constrained throughout the COVID19 crisis.

Climate-related hazards and compounded crisis impacts on food security

After decades of decline, the recent increase in food insecurity since 2014 is driven by conflict, economic slowdown as well as climate variability and extreme weather events. Nearly 690 million people or 9% of the world population were undernourished and about 750 million - or nearly 10% - were exposed to severe levels of food insecurity in 2019[97]. The number of people classified under

---

[89] https://reliefweb.int/sites/reliefweb.int/files/resources/MDRSY005do.pdf
[90] UNHCR and PIK, COVID-19, Displacement and Climate Change factsheet - https://www.unhcr.org/protection/environment/5ef1ea167/covid-19-displacement-climate-change.html
[91] https://www.internal-displacement.org/expert-opinion/tropical-cyclone-harold-and-covid-19-a-double-blow-to-the-pacific-islands
[92] Millership, 2020 cited in World Disasters Report 2020, p 18
[93] Ibid.
[94] UNOCHA Asia Pacific Humanitarian Update, Philippines Emergency Response, 20 May 2020. https://reports.unocha.org/en/country/asia-pacific/card/tjXV99QVBE/
[95] DROMIC, DSWD DROMIC Terminal Report on Typhoon "Ambo", 9 July 2020 https://reliefweb.int/report/philippines/dswd-dromic-terminal-report-typhoon-ambo-09-july-2020-6pm
[96] UNOCHA Humanitarian Needs Overview https://reliefweb.int/report/el-salvador/humanitarian-needs-overview-el-salvador-guatemala-and-honduras-addendum-impact
[97] The State of Food Security and Nutrition in the World 2020. Rome, FAO. Transforming food systems for affordable healthy diets. Available at: http://www.fao.org/3/ca9692en/online/ca9692en.html

crisis, emergency and famine conditions (Integrated Food Security Phase Classification 3 or above) had increased to almost 135 million people across 55 countries[98].

In 2020, 12 out of the 20 most vulnerable countries to climate change - and with the lowest adaptive capacity - were in conflict[99,100]. The world has also witnessed 33.4 million new internal displacements across 145 countries and territories in 2019, triggered by complex socioeconomic vulnerabilities and, often concurrently occurring, environmental degradation and climate-related disasters[101]. On top of these compounded drivers of global food insecurity, the COVID-19 pandemic has added new challenges for food insecure people and food value chains around the world.
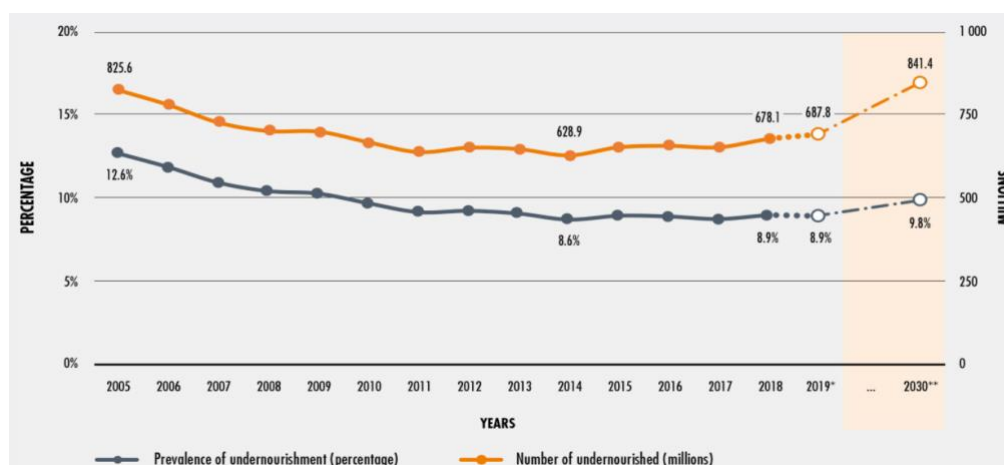

Figure 15: The number of undernourished people in the world continued to increase in 2019. Projected values in the figure are illustrated by dotted lines and empty circles. The shaded area represents projections for the longer period from 2019 to the 2030 target year. The entire series was revised to reflect new information made available since the publication of the last edition of the report; it replaces all series published previously (Source: FAO)

In 2020, over 50 million people have been doubly hit: by climate-related disasters (floods, droughts and storms) and the COVID-19 pandemic[102]. Countries in Central America are suffering from the triple-impact of hurricanes Eta and Iota, COVID-19 and pre-existing humanitarian crises. The Government of Honduras estimated that 2.8 million people were affected by hurricane Eta, and 53 000 hectares of cropland were washed away, mainly rice, beans, and sugarcane[103]. Among the Pacific Islands, tropical cyclone Harold has affected over 17 500 hectares of cropland in Vanuatu, causing substantial damage just as the growing season began[104]. Heavy rains in the Arabian Peninsula and East Africa resulted in the largest desert locust outbreak in 25 years across the Horn of Africa. In Ethiopia alone, 200 000 hectares of cropland were damaged and over 356 000 tons of cereals were lost, leaving almost one million people food insecure[105]. The long period of dry weather already observed in South America in 2020 is likely to continue as La Niña often brings below-average precipitation to some areas. As a result, corn production in Argentina is forecast to drop by 2 million tons (5% decline) in 2020-2021[106].

---

[98] 2020-Global report on food crisis. Available at: https://docs.wfp.org/api/documents/WFP-0000114546/download/
[99] ND-GAIN country index. Available at: https://gain.nd.edu/our-work/country-index/rankings/
[100] Climate Change and conflict. Available at: https://www.icrc.org/en/what-we-do/climate-change-conflict
[101] Global Report on Internal Displacement 2020. Available at: https://www.internal-displacement.org/global-report/grid2020/
[102] International Federation of Red Cross and Red Crescent Societies https://media.ifrc.org/ifrc/wp-content/uploads/2020/11/20201116_WorldDisasters_Full.pdf . News. Available at: https://media.ifrc.org/ifrc/press-release
[103] COPECO 2020. Reporte de estadísticas de incidente causados por el Huracán ETA. Available at: https://sigmof.icf.gob.hn/?page_id=7426
[104] The Pacific Islands: Tropical Cyclone Harold. Situation report-May 2020. Available at: http://www.fao.org/fileadmin/user_upload/emergencies/docs/Sit%20Rep_Cylone%20Harold_6May2020.pdf
[105] FAO in Ethiopia. Available at: http://www.fao.org/ethiopia/news/detail-events/en/c/1270924/
[106] USDA.2020. Global Agricultural Information network report. Available at: https://apps.fas.usda.gov/psdonline/circulars/production.pdf
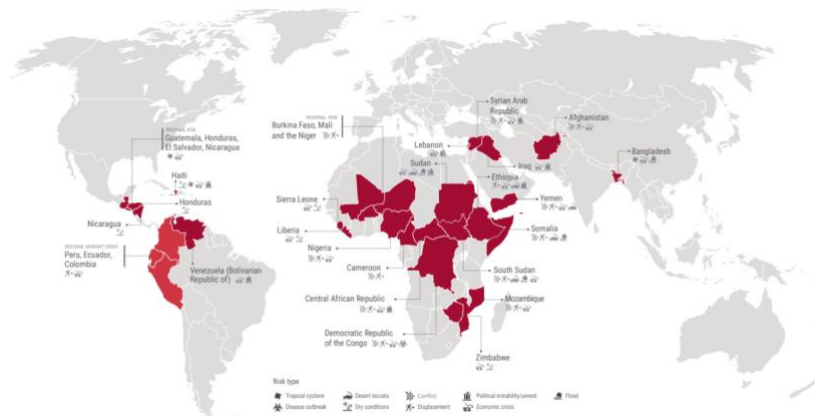
Figure 16: displays FAO-WFP early warning analysis of acute food insecurity hotspots in July 2020[107]. The hotspot countries were selected through a consensus-based analytical process by FAO and WFP, focusing primarily on: levels of food insecurity and malnutrition prior to the COVID-19 pandemic, projections of acute food insecurity, presence of existing compounding shocks and stressors, including climatic conditions, plant pests and animal diseases, economic crisis or political instability, conflict and insecurity.

The restrictions to prevent the spread of COVID-19, particularly measures to limit the movement of people within and between countries and the sale and purchase of goods and services, have posed significant challenges for managing the impacts of climate-related disasters on food insecurity. The feasibility of face-to-face services to provide farmers with information from seasonal weather forecasts as guidance on early actions has been reduced in many countries[108]. Disruptions of the agriculture sector by COVID-19 have exacerbated weather impacts along the entire food supply chain, elevating levels of food insecurity, malnutrition and undernourishment. In particular, the pandemic restrictions on movement of personnel and disruption of the supply chain of equipment has created new challenges to combat desert locust outbreaks caused by heavy rain in the Greater Horn of Africa and Yemen, where many undernourished people are currently found. Another example is Somalia. By September 2020, data suggested that the number of Somalis facing acute malnutrition (IPC Phase 3 or above) and marginally able to meet minimum food needs tripled to 3.5 million compared to early 2020[109]. Desert locusts and river floods were responsible for crop losses within the country with an estimated reduction in cereal production of 15-25% during the April-June growing season[110].

FAO's forecasts and tracking of locust swarms in the Sindh region in Pakistan, combined with local situation analysis, has helped the Government of Pakistan put effective surveillance and control operations in place. As a result, Pakistan was able to survey 61.4 million hectares and treat 1.13 million hectares of cropland now declared as locust-free zones.

---

[107] FAO-WFP 2020. FAO-WFP early warning analysis of acute food insecurity hotspots. July 2020. Data available at: http://www.fao.org/3/cb0258en/CB0258EN.pdf
[108] The dual threat of extreme weather and the COVID-19 crisis: Anticipating the impacts on food availability. Available at: http://www.fao.org/documents/card/en/c/cb0206en
[109] Food Security and Nutrition Quarterly Brief May 2020. Available at: https://www.fsnau.org/node/1756
[110] Somalia Food Security Outlook. Available at: https://fews.net/ , https://fews.net/east-africa/somalia/food-security-outlook-update/april-2020
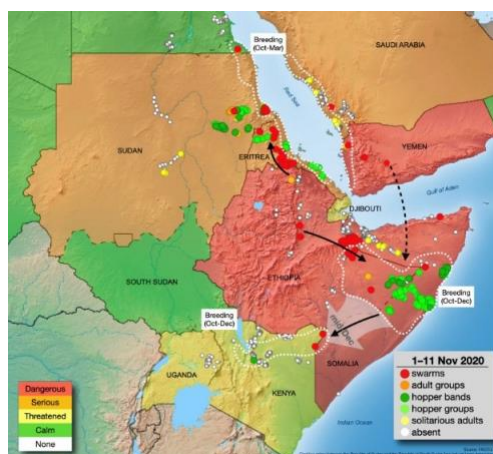
Figure 17 Desert locust movement prediction using FAO´s Desert Locust Information System (DLIS). The unusual weather conditions in fall 2019 along the Arabian Peninsula generated strong cyclones and heavy rains resulting in a higher than normal vegetation growth providing ideal conditions for desert locusts. During the 2020 compounded crisis, early warning and early action response played a key role on saving up to 1.52 million tons of cereals (enough to feed 10 million people in one year), worth around US$456 million, across nine eastern African countries and Yemen[111]. Other anticipatory actions promoted by the FAO include: i) providing key inputs to the most food insecure farmers, including seeds and agricultural tools to allow timely planting; ii) implementing cash-based programs; iii) distributing animal feed and mineral supplements to vulnerable livestock raisers; iv) monitoring and controlling all infested/breeding areas, enhancing surveillance and conducting control operations to prevent swarms from forming and spreading[112].

Sidebar: Clean energy, disaster-proof infrastructure and early warning systems

Meeting the aim of the 2015 Paris Agreement[113] "*to strengthen the global response to the threat of climate change by keeping a global temperature rise this century well below 2 degrees Celsius above pre-industrial levels and to pursue efforts to limit the temperature increase even further to 1.5 degrees Celsius*", requires sizeable reductions in carbon emissions. The International Monetary Fund in the October 2020 World Economic Outlook shows that a push in green infrastructure investment combined with steadily rising carbon prices could deliver the emission reductions needed to limit the increase in temperatures and to put the global economy on a more sustainable growth path.

Climate change mitigation policies—such as emission limits, emission trading programs, feed-in tariffs that provide a guaranteed price for producers of renewable energy, carbon taxes, and R&D subsidies—have gradually become more popular over time (Figure 18a). The introduction of environmental policies has been accompanied by increases in global innovation and investment in clean energy technologies (Figure 18b) and has made important contributions to reallocation of innovation, electricity generation, and employment towards low-carbon activities (Figure 18c-e).

A further green infrastructure investment push and subsidies for renewable energy generation, combined with pre-announced gradually increasing carbon prices, would lead to emissions reductions that are needed to keep temperature increases to safer levels (Figure 18). In turn, targeted support for the poorer households and policies that facilitate job reallocation from high-carbon to low-carbon sectors would ensure a fair transition. The costs of the transition to a low-carbon global economy are manageable, with green investment boosting economic activity and employment and thus compensating for some of the costs associated with carbon taxes.

---

[111] Desert locust upsurge – Progress report on the response in the Greater Horn of Africa and Yemen (May–August 2020). Rome. Available at: http://www.fao.org/3/cb1500en/cb1500en.pdf

[112] Early Warning Early Action Report on food security and agriculture (April–June 2020). Rome. Available at: http://www.fao.org/3/ca8606en/CA8606EN.pdf

[113] https://unfccc.int/process-and-meetings/the-paris-agreement/the-paris-agreement

While the current global recession caused by the COVID-19 pandemic can make it challenging to enact the policies needed for mitigation, it also presents opportunities to put the economy on a greener path by providing correct price signals and other financial incentives in order to boost investment into green and resilient public infrastructure, thus supporting GDP and employment during the recovery phase.
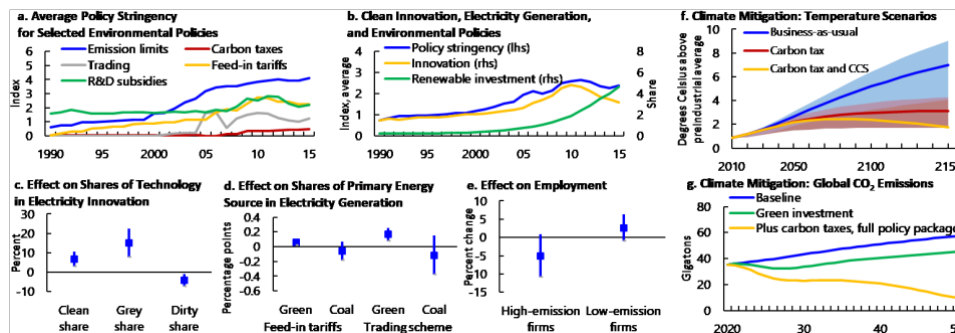

Figure 18: Impact of climate change mitigation policies. Sources: IMF (2020b); International Energy Agency; OECD Environmental Policy Stringency Index; and Worldwide Patent Statistical Database. Note: In panels c, d, e whiskers represent 90 percent confidence intervals. In panel f shaded areas represent high and low climate sensitivity. CCS = carbon capture and storage. See IMF (2020b) for full details.

Adaptation policies aimed at enhancing resilience to a changing climate—policies such as investment in disaster-proof infrastructure and early warning systems, risk sharing through financial markets, and development of social safety nets—can limit the impact of weather-related shocks and help the economy recover faster (IMF 2017). Adaptation strategies play a key role in countries that are particularly vulnerable to climate change, such as low-income countries located in hot regions and areas exposed to more frequent or severe natural disaster risks.
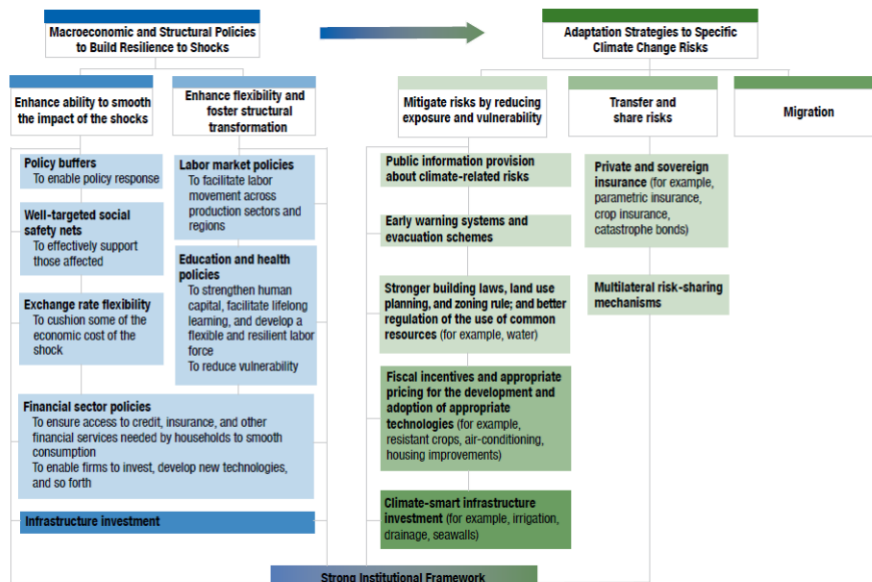

Figure 19 Climate change adaptation policies toolkit, Source IMF (2017)

Cantelmo, Alessandro, Giovanni Melina, and Chris Papageorgiou. October 2019. Macroeconomic Outcomes in Disaster-Prone Countries. International Monetary Fund Working Paper 19/217. https://www.imf.org/en/Publications/WP/Issues/2019/10/11/Macroeconomic-Outcomes-in-Disaster-Prone-Countries-48704

OECD. 2020. Environmental policy: Environmental Policy Stringency index, OECD Environment Statistics (database), https://doi.org/10.1787/2bc0bb80-en

International Monetary Fund, 2017: World Economic Outlook, October 2017. Seeking Sustainable Growth: Short-Term Recovery, Long-Term Challenges, Chapter 3, The Effects of Weather Shocks on Economic Activity: How Can Low-Income Countries Cope? https://www.imf.org/en/Publications/WEO/Issues/2017/09/19/world-economic-outlook-october-2017

International Monetary Fund, 2019: Fiscal Monitor, October 2019. Mitigating Climate Change. https://www.imf.org/en/Publications/FM/Issues/2019/09/12/fiscal-monitor-october-2019

International Monetary Fund, 2020a: Sub-Saharan Africa Regional Economic Outlook, April 2020. COVID-19: An Unprecedented Threat to Development, Chapter 2, Adapting to Climate Change in Sub-Saharan Africa, https://www.imf.org/en/Publications/REO/SSA/Issues/2020/04/01/sreo0420

International Monetary Fund, 2020b: World Economic Outlook, October 2020. A Long and Difficult Ascent, Chapter 3, Mitigating Climate Change—Growth- and Distribution-Friendly Strategies, https://www.imf.org/en/Publications/WEO/Issues/2020/09/30/world-economic-outlook-october-2020

Contributors

WMO member contributions

Algeria, Argentina, Armenia, Austria, Bahrain, Belarus, Bosnia and Herzegovina, Brazil, Bulgaria, Burkina Faso, Cameroon, Canada, Chile, China, Congo, Costa Rica, Côte d'Ivoire, Croatia, Cyprus, Czech Republic, Denmark, Estonia, Finland, France, Georgia, Germany, Greece, Guatemala; Hong Kong, China; India, Indonesia, Ireland, Israel, Italy, Japan, Jordan, Kazakhstan, Libya, Lithuania, Luxembourg, Mali, Mauritius, Moldova, Netherlands, New Zealand, Norway, Pakistan, Paraguay, Peru, Poland, Romania, Russia, Saudi Arabia, Senegal, Serbia, Singapore, Slovakia, Slovenia, South Africa, South Korea, Spain, Sudan, Sweden, Switzerland, Tunisia, Turkey, Ukraine, United Kingdom, USA, Uzbekistan, WMO RA VI Regional Climate Centre (RCC).

Individual contributors

Signe Aaboe (MET Norway), Jorge Alvar-Beltrán (FAO), Jana Birner (UNHCR), Jessica Blunden (NOAA National Centers for Environmental Information), Tim Boyer (NOAA's National Centers for Environmental Information), Anny Cazenave (Laboratoire d'Etudes en Géophysique et Océanographie Spatiales CNES and Observatoire Midi-Pyrénées, France), Lijing Cheng (Institute of Atmospheric Physics, Chinese Academy of Sciences, China; and Center for Ocean Mega-Science, Chinese Academy of Sciences, Qingdao, China, 266071), Jocelyn Christine Turnbull (National Isotope Centre, GNS Science, New Zealand), Andrew Crotwell (NOAA, USA), Damien Desbruyères (Ifremer, University of Brest, CNRS, IRD, Laboratoire d'Océanographie Physique et Spatiale, France), Catia Domingues (National Oceanographic Centre, UK; and ARC Centre of Excellence for Climate Extremes, University of Tasmania, Hobart, Tasmania, Australia), Edward Dlugokencky (NOAA, USA), Simon Eggleston (WMO), Christoph Gerbig (Max-Planck Institute for Biogeochemistry, Germany), John Gilson (University of California, USA), Luke Gregor (ETZH), David Griffith (University of Wollongong, Australia), Lorenzo Guadagno (IOM), Brad Hall (NOAA, USA), Valentine Haran (Visiting Scientist at WMO, University of Geneva), Ana Heureux (FAO), Sander Houweling (SRON, the Netherlands), Matthias Huss (ETH Zürich), Aamer Irshad (FAO), Masayoshi Ishii (Department of Atmosphere, Ocean and Earth System Modeling Research, Meteorological Research Institute, Japan), Kirsten Isensee (IOC UNESCO), Gregory C. Johnson (NOAA, Pacific Marine Environmental Laboratory, USA), Armin Jordan (Max-Planck Institute for Biogeochemistry, Germany), Maarten Kappelle (UNEP), John Kennedy (UK Met Office), Rachel Killick (Met Office Hadley Centre, UK), Brian A. King (National Oceanographic Centre, UK), Nicolas Kolodziejczyk (University of Brest, CNRS, IRD, Ifremer, Laboratoire d'Océanographie Physique et Spatiale, IUEM, France), Paul Krummel (CSIRO, Australia) Thomas Lavergne (MET Norway), Haeyoung Lee (KMA, Republic of Korea), Zoë Miranda Loh (CSIRO, Australia), John Lyman (NOAA, Pacific Marine Environmental Laboratory, USA), Nicholas Middleton (UNEP), Maeva Monier (CELAD/Mercator Ocean International, France), Didier Paolo Monselesan (CSIRO Oceans and Atmosphere, Hobart, Tasmania, Australia), Lorena Moreira (International Space Science Institute, Bern), Lev Neretin (FAO), Giorgia Pergolini (WFP), Anne Olhoff (UNEP-DTU Partnership UDP), Evgenia Pugacheva (IMF), Claire Ransom (Visiting Scientist at WMO, Institut de Hautes Etudes Internationales et du Development), Dean Roemmich (Scripps Institution of Oceanography, UCSD, San Diego, CA, USA), Yousuke Sawa (JMA, Japan), Robert Schlegel (Institut de la Mer de Villefranche (IMEV), France), Tina Schoolmeester (GRID Arendal), Katherina Schoo (IOC UNESCO), Ria Sen (WFP), Martin Stendel (DMI), Faisal Syed (FAO), Oksana Tarasova (WMO Secretariat), Blair Trewin (Bureau of Meteorology, Australia), Freja Vamborg (ECMWF), Alex Vermuelen (ICOS Carbon Portal, Sweden), Karina von Schuckmann (Mercator Ocean international, France), Ying Wang (UNEP), Ray Weiss (Scripps Institution of Oceanography, USA), Susan E. Wijffels (CSIRO Oceans and Atmosphere, Hobart, Tasmania, Australia; and Woods Hole Oceanographic Institution, Massachusetts, United States), Michelle Yonetani (UNHCR), Markus Ziese (Deutscher Wetterdienst, Germany).

Data set details

Temperature data

Global mean temperature is reported as the mean of five data sets listed below. Global mean temperature anomalies are expressed relative to the 1850-1900 average. However, only HadCRUT goes back to 1850. The averages for the NOAAGlobalTemp and GISTEMP data set are set equal to that of HadCRUT over the period 1880-1900 and averages for the two reanalyses are set to equal that of HadCRUT over the period 1981-2010.

HadCRUT.4.6.0.0: Morice, C. P. et al., 2012: Quantifying uncertainties in global and regional temperature change using an ensemble of observational estimates: The HadCRUT4 dataset, Journal of Geophysical Research, 117, doi:10.1029/2011JD017187.

NOAAGlobalTemp v5: Zhang, H.-M., B. Huang, J. Lawrimore, M. Menne, Thomas M. Smith, NOAA Global Surface Temperature Dataset (NOAAGlobalTemp), Version 4.0 [indicate subset used]. NOAA National Centers for Environmental Information. doi:10.7289/V5FN144H [access date].

Huang, B., and Coauthors, 2020: Uncertainty Estimates for Sea Surface Temperature and Land Surface Air Temperature in NOAAGlobalTemp Version 5. J. Climate, 33, 1351–1379, https://doi.org/10.1175/JCLI-D-19-0395.1.

GISTEMP v4: GISTEMP Team, 2019: GISS Surface Temperature Analysis (GISTEMP), version 4. NASA Goddard Institute for Space Studies, https://data.giss.nasa.gov/gistemp/.

Lenssen, N. et al., 2019: Improvements in the GISTEMP uncertainty model. Journal of Geophysical Research: Atmospheres, 124 (12), doi:10.1029/2018JD029522.

ERA5: Hersbach, H, Bell, B, Berrisford, P, et al. The ERA5 global reanalysis. Q J R Meteorol Soc. 2020; 146: 1999– 2049. https://doi.org/10.1002/qj.3803

JRA-55: Kobayashi, S. et al., 2015: The JRA-55 reanalysis: General specifications and basic characteristics. Journal of the Meteorological Society of Japan. Ser. II, 93(1)

Greenhouse gas data

Estimated concentration from 1750 are used to represent pre-industrial conditions. Calculation assume a pre-industrial mole fraction of 278 ppm for CO_2, 722 ppb for CH_4 and 270 ppb for N_2O.

WMO Greenhouse Gas Bulletin, No.16, November 2020, https://library.wmo.int/index.php?lvl=notice_display&id=21795#.X7v7lM1KhPY

Ocean heat content data

Cheng, L., Trenberth, K. E., Fasullo, J., Boyer, T., Abraham, J., & Zhu, J. (2017). Improved estimates of ocean heat content from 1960 to 2015. *Science Advances*, *3*(3), e1601545. https://doi.org/10.1126/sciadv.1601545

CMEMS (CORA, http://marine.copernicus.eu/science-learning/ocean-monitoring-indicators)

Desbruyères, D. G., Purkey, S. G., McDonagh, E. L., Johnson, G. C., & King, B. A. (2016). Deep and abyssal ocean warming from 35 years of repeat hydrography. *Geophysical Research Letters*, *43*(19), 10, 310–356, 365. https://doi.org/10.1002/2016GL070413

Domingues, C. M., Church, J. A., White, N. J., Gleckler, P. J., Wijffels, S. E., Barker, P. M., & Dunn, J. R. (2008). Improved estimates of upper-ocean warming and multi-decadal sea-level rise. *Nature*, *453*(7198), 1090–1093. https://doi.org/10.1038/nature07080

Gaillard, F., Reynaud, T., Thierry, V., Kolodziejczyk, N., & von Schuckmann, K. (2016). In Situ–Based Reanalysis of the Global Ocean Temperature and Salinity with ISAS: Variability of the Heat Content and Steric Height. Journal of Climate, 29(4), 1305–1323. https://doi.org/10.1175/JCLI-D-15-0028.1

Good, S. A., Martin, M. J., & Rayner, N. A. (2013). EN4: Quality controlled ocean temperature and salinity profiles and monthly objective analyses with uncertainty estimates. Journal of Geophysical Research: Oceans, 118(12), 6704–6716. https://doi.org/10.1002/2013JC009067

Hosoda, S., Ohira, T., & Nakamura, T. (2008). A monthly mean dataset of global oceanic temperature and salinity derived from Argo float observations. JAMSTEC Report of Research and Development, 8, 47–59. https://doi.org/10.5918/jamstecr.8.47

Ishii, M., Fukuda, Y., Hirahara, S., Yasui, S., Suzuki, T., & Sato, K. (2017). Accuracy of Global Upper Ocean Heat Content Estimation Expected from Present Observational Data Sets. SOLA, 13, 163–167. https://doi.org/10.2151/sola.2017-030

IPRC (http://apdrc.soest.hawaii.edu/projects/Argo/)

Levitus, S., Antonov, J. I., Boyer, T. P., Baranova, O. K., Garcia, H. E., Locarnini, R. A., Mishonov, A. V, Reagan, J. R., Seidov, D., Yarosh, E. S., & Zweng, M. M. (2012). World ocean heat content and thermosteric sea level change (0–2000 m), 1955–2010. Geophysical Research Letters, 39(10). https://doi.org/10.1029/2012GL051106

Li, H., Xu, F., Zhou, W., Wang, D., Wright, J. S., Liu, Z., & Lin, Y. (2017). Development of a global gridded Argo data set with Barnes successive corrections. Journal of Geophysical Research: Oceans, 122(2), 866–889. https://doi.org/10.1002/2016JC012285

Lyman, J. M., & Johnson, G. C. (2014). Estimating Global Ocean Heat Content Changes in the Upper 1800 m since 1950 and the Influence of Climatology Choice. Journal of Climate, 27(5), 1945–1957. https://doi.org/10.1175/JCLI-D-12-00752.1

Roemmich, D., & Gilson, J. (2009). The 2004–2008 mean and annual cycle of temperature, salinity, and steric height in the global ocean from the Argo Program. Progress in Oceanography, 82(2), 81–100. https://doi.org/https://doi.org/10.1016/j.pocean.2009.03.004

Roemmich, D., Church, J., Gilson, J., Monselesan, D., Sutton, P., & Wijffels, S. (2015). Unabated planetary warming and its ocean structure since 2006. Nature Climate Change, 5, 240.

von Schuckmann, K., & Le Traon, P.-Y. (2011). How well can we derive Global Ocean Indicators from Argo data? Ocean Sci., 7(6), 783–791. https://doi.org/10.5194/os-7-783-2011

Sea level data

Archiving, Validation and Interpretation of Satellite Oceanographic data (AVISO): Legeais, J.-F. et al., 2018: An improved and homogeneous altimeter sea level record from the ESA Climate Change Initiative. Earth System Science Data, 10, doi: 10.5194/essd-10-281-2018

Copernicus Marine Environment Monitoring Service (CMEMS): Pujol, M.-I. et al., 2016: DUACS DT2014: the new multi-mission altimeter data set reprocessed over 20 years. Ocean Science, 12, doi: 10.5194/os-12-1067-2016, 2016.

Ablain, M. et al, 2017: Satellite altimetry-based sea level at global and regional scales. Surveys in Geophysics, 38, doi: 10.1007/s10712-016-9389-8.

Escudier, P. A. et al., 2017: Satellite radar altimetry: principle, accuracy and precision. In Satellite Altimetry Over Oceans and Land Surfaces (D. Stammer and A. Cazenave, eds)

Marine heatwave data

MHWs are categorized as follows: moderate, when the sea-surface temperature is above the 90th percentile of the climatological distribution for five days or longer (Hobday et al. 2018); strong, if the difference from the long-term average is more than twice that between the 90th percentile and the long-term mean; severe, if the difference from the long-term average is more than three times as large, and extreme, if that difference is more than four times as large.

Hobday, A.J. et al., 2018: Categorizing and naming marine heatwaves. Oceanography 31(2), doi.org/10[.]5670/oceanog.2018.205

NOAA OISST v2: Optimum Interpolation Sea Surface Temperature (OISST) Banzon, V. et al.,2016: A long-term record of blended satellite and in situ sea-surface temperature for climate monitoring, modeling and environmental studies. Earth System Science Data, 8, doi:10.5194/essd-8-165-2016

Ocean acidification data

Data from sampling sites were extracted from the 14.3.1 data portal (http://oa.iode.org) for the time period from 1 January 2010 to 8 January 2020. Annual averages, maxs and mins were calculated for each station for each year.

The global pH data set is based on a variety of oceanographic variables:

CMEMS
https://resources.marine.copernicus.eu/?option=com_csw&view=details&product_id=GLOBAL_OMI_HEALTH_carbon_ph_area_averaged

Sea ice data

Data set background: The sea ice section uses data from the EUMETSAT OSI SAF Sea Ice Index v2.1 data set (Lavergne et al., 2019) and the NSIDC v3 Sea Ice Index (Fetterer et al., 2017). Sea ice concentrations are estimated from microwave radiances measured from satellites. Extent is calculated as the area of ocean grid cells where the sea-ice concentration exceeds 15%. Although there are relatively large differences in the absolute extent between data sets, they agree well on the year-to-year changes and the trends. In this report, NSIDC are reported for absolute extents (e.g. "18.95 million km^2") for consistency with earlier reports, while rankings are reported for both data sets.

Fetterer, F., K. Knowles, W. N. Meier, M. Savoie, and A. K. Windnagel. 2017, updated daily. Sea Ice Index, Version 3. Boulder, Colorado USA. NSIDC: National Snow and Ice Data Center. doi: https://doi.org/10.7265/N5K072F8. Accessed Oct. 2020.

Lavergne, T., Sørensen, A. M., Kern, S., Tonboe, R., Notz, D., Aaboe, S., Bell, L., Dybkjær, G., Eastwood, S., Gabarro, C., Heygster, G., Killie, M. A., Brandt Kreiner, M., Lavelle, J., Saldo, R., Sandven, S., and Pedersen, L. T.: Version 2 of the EUMETSAT OSI SAF and ESA CCI sea-ice concentration climate data records, The Cryosphere, 13, 49–78, https://doi.org/10.5194/tc-13-49-2019, 2019.

Greenland ice sheet data

Data are from the Polar Portal http://polarportal.dk/en/home/

The ice discharge series is derived from satellite data which can be used to measure glacier flow speeds all around the edges and is available since 1986. This is used to estimate how much ice is being lost as icebergs.

Slightly different models have been used to calculate the Surface Mass Balance (SMB) over time which, with different forcing data, may give slightly different results.

Precipitation data

The following Global Precipitation Climatology Centre (GPCC) data sets were used in the analysis:

- First Guess Monthly, DOI: 10.5676/DWD_GPCC/FG_M_100
- Monitoring Product (Version 6), DOI: 10.5676/DWD_GPCC/MP_M_V6_100
- Full Data Monthly (Version 2018), DOI: 10.5676/DWD_GPCC/FD_M_V2018_100
- First Guess Daily, DOI: 10.5676/DWD_GPCC/FG_D_100
- Full Data Daily (Version 2018), DOI: 10.5676/DWD_GPCC/FD_D_V2018_100

Arctic sidebar data

The Arctic sidebar is based on data from other sections within the statement, on information from regional and country reports, as well as on the following datasets:

Copernicus Climate Change Service3S ERA5 temperature dataset. Described in Hersbach, H, Bell, B, Berrisford, P, et al. The ERA5 global reanalysis. Q J R Meteorol Soc. 2020; 146: 1999– 2049. https://doi.org/10.1002/qj.3803, available at - https://cds.climate.copernicus.eu/cdsapp#!/dataset/ecv-for-climate-change?tab=overview

Copernicus Atmosphere Monitoring Service Global Fire Assimilation System (GFAS) https://confluence.ecmwf.int/display/CKB/CAMS%3A+Global+Fire+Assimilation+System+%28GFAS%29+data+documentation

CAMS wildfire emission dataset and interpretation thereof https://atmosphere.copernicus.eu/copernicus-reveals-summer-2020s-arctic-wildfires-set-new-emission-records#

Precipitation – see Precipitation data section

Sea ice – see Sea ice data section

Marine heatwaves – See marine heatwave section